hoofdgroep
maatschappelijke technologie

organisatie voor
toegepast-natuurwetenschappelijk
onderzoek

DATA REPORT

THE WAKE OF A HORIZONTAL-AXIS WIND TURBINE MODEL; MEASUREMENTS IN UNIFORM APPROACH FLOW AND IN A SIMULATED ATMOSPHERIC BOUNDARY LAYER

by

A.M. Talmon

TNO

postbus 342
7300 AH apeldoorn

bezoekadres
laan van westenenk 501

telex 36395 tnoap
telefoon 055 - 77 33 44

Ref. nr. : 85-010121
File nr. : 8724-12433
Date : August 1985
NP

Keywords:

wind energy
wind turbine
wake effects

ST code : C 19-3

For:

P.E.O.
Leidsche Veer 35
3511 SB Utrecht

Project no. 4401
Job no. 8.8.3

CONTENTS Page

LIST OF SYMBOLS

		dimension
A	surface area of rotordise or tower	m^2
a,b	constants	
C_T	drag coefficient	
C_P	power coefficient	
D	rotor diameter	m
F	force	N
n	frequency	Hz
P	power	W
R	radius rotor	m
Re	Reynolds number	
$S_{uu}(n)$	power spectral density	m^2/s
U V W	velocity components	m/s
u' v' w'	rms values of velocity components	m/s
$\bar{U}$	mean value of velocity component	m/s
$\bar{U}_r$	mean velocity at reference locations	m/s
$\Delta\bar{U}$	velocity defect	m/s
$\Delta\bar{U}_{max}$	maximum velocity defect	m/s
$\Delta u'$	rms value above ambient level	m/s
X Y Z	coordinates	m
x_{Lu} x_{Lv} x_{Lw}	integral length scales	m
X_{NW}	near wake length	m
Z_o	roughness parameter	m
ρ	air density	kg/m^3
λ	tip speed ratio	

SUMMARY

Wake effects will cause power loss when wind turbines are grouped in so called wind turbine parks. Wind tunnel measurements of the wake of a wind turbine model are conducted in order to refine calculations of wake effects.

Wake effects caused by tower and nacelle are studied in uniform flow. Wake development depending on tip speed ratio is studied in a simulated atmospheric boundary layer.

In this data report the wind tunnel results are described.

Main conclusions are:

- Ground effects inhibit vertical growth of the lower part of the wake.
- Turbine drag and centerline velocity defects are strongly interrelated.
- The velocity defect wake profile of a wind turbine shifts slightly towards the ground.

1. INTRODUCTION

When wind turbines are grouped in wind turbine parks, wake effects will cause power loss. In order to refine calculations of wake interaction effects, tower, nacelle, ground, operating condition and ambient flow effects need to be known.

In this date report wind tunnel measurements in both uniform flow and simulated atmospheric boundary layer flow are described.

The uniform flow experiments are primarely directed towards measurement of tower and nacelle effects.
Atmospheric boundary layer flow experiments are primarely directed towards the study of operating condition effects.
Ground effects and ambient flow effects are studied in both flow cases.

The experimental arrangements are described in chapter 2.
The properties of the rotor, depending on operating conditions, are described in chapter 3. Uniform flow measurements are summarized in chapter 4. Simulated atmospheric boundary layer wake flow results are given in chapter 5. In chapter 6 results are discussed. In chapter 7 conclusions are drawn.

The uniform flow wake measurements have been reported in an earlier stage by Talmon [9] (in Dutch).

This study is part of phase 2 of the Dutch National Wind Energy program (NOW-2 project 4401 Job 8.8.3).

2. EXPERIMENTAL ARRANGEMENT

2.1 The wind turbine model(s)

The wind turbine model is constructed on the basis of a 0.36 m diameter model rotor. The rotor is described in Vermeulen [1]. The model can be equipped with a cylindrical as well as a lattice tower, resulting in a hub-height of 0.36 m. The model can also be equipped with a cylindrical nacelle or a rectangular nacelle.

Dimensions of towers and nacelles are as follow:

- cylindrical tower: diameter : 26.7 mm
  length cylinder : 330 mm
  material : steel
- lattice tower : diameter vertical legs : 4 mm
  diameter horizontal legs : 3 mm
  base plate dimensions : 94 x 94 mm^2
  top plate dimensions : 40 x 40 mm^2
- cylindrical nacelle: (= outer dimension of generator)
  diameter : 42 mm
  length : 145 mm
- rectangular nacelle: 180 x 60 x 50 mm^3

In fig. 1 the model configurations are shown.
In fig. 2 the model is placed in the wind tunnel in which the ABL flow is simulated.

2.2 The test facilities

2.2.1 Uniform flow

Uniform approach flow measurements have been performed in the closed circuit MIA wind tunnel (cross-section 2.7 x 1.2 m^2), see Builtjes [2]. The smooth empty tunnel is equipped with an anti-turbulence gause at the entrance of the measuring section.

Drag and power of the rotor are measured with the rotor at a height of 0.6 m above the wind tunnel floor. The test rig is the same as used by Vermeulen [1] with a strain gauge balance placed on top of it.

In the case of wake flow measurements the tunnel is equipped with a hydraulically smooth false floor, length 4.5 m. The round shaped upstream edge of the false floor is located 0.5 m downstream of the anti-turbulence gauze. The wind turbine model is placed 0.5 m downstream of the upstream edge of the false floor.

Properties of the flow are discussed in section 4.

2.2.2 Simulated Atmosferic Boundary Layer (A.B.L.) flow

Wake flow measurements under simulated ABL flow conditions are performed in an open circuit wind tunnel with cross section 2 x 3 m^2, see fig. 3.
In front of the 16 m long entrance section a barriere of 0.3 m height is placed to generate the ABL flow. The ABL is simulated on a scale of 1 : 250. The tunnel is equipped with a rough carpet which simulates approach flow over rural terrain ($Z_o \cong 0.1$ m).

Properties of the ABL flow are discussed in section 5.

2.3 Instrumentation

2.3.1 Rotor speed control unit

The wind turbine rotor is kept at constant speed by an electronic circuit. Basically the circuit generates a counter rotating magnetic field in the generator. A tacho generator is also located on the rotor axis. The circuit monitors the voltage of the tacho generator. Deviations from the set point value, which corresponds to the desired rotor speed, are adjusted by control of the magnetic field.
Except for the wake measurements in uniform flow use is made of a new commercial available control unit which operates at high accuracy (Aerotech 93084).

2.3.2 Drag measurements

Drag measurements are performed with a one-component strain gauge balance orientated in mean flow direction.
The balance is located beneath the wind turbine models, flush mounted in wind tunnel floor or false floor.

2.3.3 Power measurement

The power necessary to keep the rotor at constant speed is calculated by measuring simultaneous mean generator current and mean generator voltage (the rotor control unit operates in DC mode). After correction for rotor bearing losses, the power generated by the rotor is obtained.

2.3.4 Velocity measurements

Mean velocity measurements in the uniform flow are performed with a pitot tube of 3 mm diameter and a Schlumberger (CA 1065 + CH 5112/0) differential pressure transducer ± 2 mbar.

Velocity measurements in the ABL flow are performed with two-component hot-wire anemometers.
Signals are digitized, stored and processed by computer.

equipment:	probes	DISA 55P53 55P54
	anemometer	DISA/DANTEC 56G01 CTA
	storage	Preston GMAD-4A
	computer	HP 1000-F

2.3.5 Measuring mean values of signals

Two TNO built voltage to frequency converter type voltmeters are used to determine mean drag, power and pressure difference (in case of pitot-tube measurements). Averaging periods in the uniform flow are 30 s. In the ABL flow averaging periods are 60 s.

3. PROPERTIES OF THE WIND TURBINE ROTOR

3.1 Rotor performance in uniform flow

The profile of the rotor blades is a Göttingen type Gö 804, see Vermeulen [1]. Power measurements in the special case of a simulated ABL + anti-turbulence gauze are given in Vermeulen [1].
Drag measurements in low turbulence uniform approach flow are given in Vermeulen [3].

The performance of the rotor is checked by repeating the experiments of Vermeulen, with three slightly different free stream velocities. The experiments are done in the MIA tunnel, as described in section 2.2.1. The free stream velocity is measured at hub height, two rotor-diameters to the side of the rotor centerline.

The drag is expressed by the drag coefficient: $C_T = \frac{F}{\frac{1}{2}\rho\bar{U}^2 A}$

The power is expressed as: $C_p = \frac{P}{\frac{1}{2}\rho\bar{U}^3 A}$

Free stream velocities are: $\bar{U}$ = 8.6, 9.7, 11.8 m/s.

Results are shown in figures 4, 5 and 6. The drag coefficient is independent of free stream velocity.
In the power curve a slight change with free stream velocity is shown. This is probably caused by a Reynolds dependence of the flow around the blades.

3.2 Rotor performance in the ABL flow

The properties of the ABL flow are described in section 5.2.
The wind turbine model is equipped with a cylindrical tower and nacelle. Free stream velocity at hub height is approximately 9.7 m/s.
Measurement of rotor power is performed as described in section 2.3.3. The drag balance is located in the tunnel floor. The cylindrical tower is isolated from the surrounding wind by constructing a cylindrical protection shield around the tower. That way the balance measures only the forces acting on the rotor.

Results are shown in fig. 7. Comparing the results with fig. 5 shows no influence of the ABL flow on C_T. In the ABL a slight power loss seems to be appearend.

4. THE WAKE IN UNIFORM FLOW

The wake of the .36 m model rotor has been previously measured by Vermeulen [1] in another wind tunnel under slightly different flow conditions. In those experiments the rotor centerline was located at the tunnel centerline, so the rotor wake did not touch ground or wind tunnel walls.

In the present experiments the rotor centerline is located .36 m above ground. The model is equipped with different combinations of towers and nacelles.

In this capter results of the present experiments are given.
The coordinate system used is depicted in fig. 8.

4.1 Proporties of approach flow

The mean velocity (U ~ 9.6 m/s) is measured in absence of the wind turbine model. Results of horizontal traverses on Z = .36 m height are given in fig. 9. Results of vertical tracerses with Y = 0 are given in fig. 10. In horizontal direction (- 0.5 Y/D, 0.5 Y/D) a velocity difference of 0.5% is appearend. In vertical direction a velocity difference of 3% is measured.

Turbulence intensities are:

X direction 0.4 à 0.5%
Y direction 0.4 à 0.5%

4.2 Properties of the towers

The drag of the towers is measured by placing the towers on the strain gauge balance. The drag coefficients are determined over a free stream velocity range of 8 to 18 m/s. Results are shown in table 1. The drag coefficient of the cylindrical tower is in correspondence with the value expected C_T = 1.2, Re ~ 3.10^5, see Vermeulen [4].

The wakes of different combinations of tower and nacelles are shown in fig. 11.

4.3 Drag of the wind turbine models

The drag of the wind turbine models is also measured. Results are spurious; too much drag is measured. Checking electronics revealed a malfunction of an amplifier. During the measurements of C_P and C_T of the rotor alone another amplifier is used (fig. 4 - 7).
An upperbound of the drag of the models can be calculated by summation of rotor drag and tower drag (table 1).

4.4 The wake of the wind turbine models

4.4.1 Model configurations

Four configurations are used.

A	-	cylindrical	tower	+	cylindrical nacelle	●
B	-	cylindrical	"	+	rectangular "	□
C	-	lattice	"	+	cylindrical "	o
D	-	lattice	"	+	rectangular "	★

Models are shown in fig. 1.

4.4.2 Experimental procedure

The rotor is operated at a tipspeed ratio of $\lambda = 6.4$.
The flow velocity outside the wake is slightly higher than in absence of the wind turbine model.
The velocity outside the wake is measured at positions (X, -2.08 D, 0). This velocity is called the reference velocity $\bar{U}_r$. It is needed to determine velocity defects in the wakes, making it a substiantial part of the wake traverse procedure.

Preliminary measurements indicated a downshift of the location of maximum velocity defect. The experimental procedure used in conducting radial wake traverses at fixed X-locations (X/D = 2, 5, 9.6), is as follow:

a - $\bar{U}_r$ is measured
- A vertical traverse at Y = 0 is made
- $\bar{U}_r$ is measured
- The location of maximum velocity defect is determined

b - $\bar{U}_r$ is measured
- A horizontal traverse through the location of maximum velocity defect
- $\bar{U}_r$ is measured

To determine the maximum velocity defect at several downstream X-locations longitudinal wake traverses are performed as follow:

At each downstream location $\bar{U}_r$ is measured. In the vertical plane (Y = 0) a small vertical traverse at hub-height is used in search for the maximum velocity defect.

4.4.3 Results

Characteristic parameters of a wake traverse are:

- The maximum velocity defect : $\Delta\bar{U}_{max}$
- Half the maximum velocity defect: $\frac{1}{2}\Delta\bar{U}_{max}$
- The location of $\Delta\bar{U}_{max}$
- The location of points $\frac{1}{2}\Delta\bar{U}_{max}$

Results of the vertical wake traverses for all four model configurations are shown in fig. 12. Displacement of the wake towards the ground is observed. Locations of $\Delta\bar{U}_{max}$ en $\frac{1}{2}\Delta\bar{U}_{max}$ are shown in fig. 13 and table 2.

Results of horizontal wake traverses for model configuration A are shown in figure 14. Horizontal wake traverses at X/D = 9.6 are shown in fig. 15. Locations of $\Delta\bar{U}_{max}$ en $\frac{1}{2}\Delta\bar{U}_{max}$ are shown in fig. 16 and table 12.

Results of longitudinal wake traverses are shown in fig. 17.

5. THE WAKE IN THE SIMULATED ABL FLOW

5.1 ABL flow measurement

The tunnel is described in section 2.2.2. Two-component hot-wire probes are used to measure the ABL flow. The measurements are to be used as a basis for calculating mean velocity wake defects. At Z = 0.352 m above the floor, which is the hub-height of the rotor, the mean flow velocity is 9.7 m/s. At hub-height horizontal traverses are made at X/D = 0, 2, 4 and 7. Vertical traverses are also made at X/D = 0, 2, 4 and 7.

The hot-wire probes signals are sampled at a rate of 65 Hz giving measuring periods of 30 s. Per measuring location two measurements of 30 s duration are made. This yields a measuring period of 60 s for $\bar{U}$. Other results, such as u' v' or spectra, are mean values of two 30 s measuring periods.

5.2 ABL flow results

The ABL flow results are described in an coordinate system which is located at the wind tunnel floor.

Horizontal traverses at hub-height, over $-1{,}67 < Y/D < 1.67$, show no significant deviations of $\bar{U}$, u' and v' from an uniform distribution. Horizontal profiles are in the following assumed to be uniform.
Vertical traverses, over $0.022 < Z < 1.100$ m, show logaritmic profiles. The vertical profile at X/D = 0 is shown in fig. 18. The roughness parameter Z_o is calculated from this profile, using locations up to 0.15 m above the floor, resulting in $Z_o = 0.6\ 10^{-3}$ m. On a scale of 1 : 250 this is equal to $Z_o = 0.15$ m. This is slightly rougher than open farmland.

Turbulence intensities, spectra and length scales are shown in figures 19 to 21 (spectra of u, v and w lie in the same band). Definitions are according to ESDU 74031 (ref. [5]). Results are summarized in table 3. For reason of comparison ESDU data is also included in these figures.

Due to the sample rate of 65 Hz, the higher frequency part of the velocity fluctuations is not included in the calculation of u', v' and w'. It is estimated from fig. 20 that accounting for this part would lead to a correction of u', v' and w' by a factor 1.02, which of course is to be neglegted.

5.3 The wake in the ABL flow

5.3.1 Rotor operating conditions

The mean velocity at hub height is fixed at 9.7 m/s. Tip speed ratios of λ = 3.5, 4.7, 6.6, 8.5 and 9.3 are used. In this case λ is defined as:

$$\lambda = \frac{2\pi \, n \, R}{\bar{U}(\text{hub height})}$$

This range of operating conditions is chosen to study operating conditions on wind turbine wake development.
At λ = 3.5 the rotor is operated at low C_T and low C_P (see fig. 7).
At λ = 6.6 the rotor is operated at normal C_T and optimum C_P.
At λ = 9.3 the rotor is operated at high C_T and very low C_P.
At λ = 4.7 and λ = 8.5 the rotor is operated at intermediate conditions. In section 3.2 C_T and C_P in ABL flow are discussed.

5.3.2 Experimental procedure

The experimental procedure is basically the same as in the uniform flow experiments. Use is made of reference points located at (X, -1.67 D, 0).
Vertical wake traverses are made at X/D = 2, 4 and 7.
By subtracting the already measured ABL vertical profiles the vertical velocity defect profile is calculated.
As in the uniform flow experiments the wake is subjected to a downshift.
The Z-location of maximum velocity defect is determined (= location of wake symmetry).
Horizontal wake profiles, at X/D = 2, 4 and 7, are made at the before determined Z-heights of maximum velocity defect, see table 4.

The magnitude of maximum velocity defect is as nearly the same as the velocity defect at hub-height. Determination of the decay of maximum velocity defect is therefore performed by longitudinal traverses at hub height.

5.3.3 Mean wake flow results

Vertical and horizontal wake traverses are made at tip-speed ratios of λ = 4.7, 6.6 and 8.5. Typical mean flow vertical profiles are shown in fig. 22 for λ = 6.6.

Vertical velocity defect profiles at X/D = 2 are shown in fig. 23.
" " " " " X/D = 4 and 7 are shown in fig. 24.
Horizontal velocity defect profiles at X/D = 2 are shown in fig. 25.
" " " " " X/D = 4 and 7 are shown in fig. 26.

Characteristic locations in the velocity defect profiles are:

$Z(\Delta\bar{U}_{max})$ = Z(symmetry), $Z(\frac{1}{2}\Delta\bar{U}_{max})$ and $Y(\frac{1}{2}\Delta\bar{U}_{max})$. In table 5 these locations are summarized.

Longitudinal traverses at rotor centerline are shown in fig. 27 and summarized in table 6.

5.3.4 Turbulent wake flow results

Turbulence intensity profiles at λ = 6.6 are shown in fig. 28. (Note: horizontal and vertical profiles of longitudinal and radial turbulence intensities are shown).
The turbulence intensity profiles are characterised by:

a. The turbulence intensity at wake centerline,
b. Turbulence excess at radial positions at approximately $|Z/D|$ and $|Y/D|$ = 0.4.

The decay of centerline turbulence is shown in fig. 29 (note: intensities at λ = 3.5 and λ = 4.5 are approximately equal, also are intensities at λ = 8.5 and 9.2).

In table 7 turbulence intensities at centerline and at radial positions are summarized. At X/D = 2 an excess of turbulence intensity is measured. At X/D = 7 the turbulence intensity is practically uniform distributed.

6. DISCUSSION OF RESULTS

6.1 Tower, Nacelle and ground effects

In this section attention is directed towards wake effects related to tower shape; nacelle shape and ground induced effects.

Tower effect:

The velocity defect caused by the tower results in an extra velocity defect measured in the lower part of the vertical traverses, fig. 12.

Tower shape effects:

1) - The drag of the lattice tower is less, section 4.2.
2) - The location of $\Delta\bar{U}_{max}$ (X/D = 2) of the lattice tower is closer to the centerline.
3) - Systematically $\Delta\bar{U}_{max}$ of the lattice tower configurations is greater, fig. 12.
4) - For Z/D < -0.5 the velocity defect of the lattice tower is less, fig. 12.

The turbine wake development is influenced by the mean velocity defect and the turbulence structure generated by the tower. Effect no. 4 is to be contributed to different mean velocity defects associated with the tower constructions (this corresponds with effect no. 1).
Effects no. 2 and 3 are probably caused by both differences in mean velocity defect and turbulence structure.

Nacelle effects:

No significant effects are measured.

Ground effect:

The vertical traverses show a wake which is shifted towards the ground. The tower effect introduces an extra velocity defect in the lower part of the wake.

Recovery from velocity defects in upper and lower parts of the wake proceed at different rates, see figure 12.
Velocity defects in the upper part of the wake decrease faster than close to the ground. The ground inhibits wake decay by limiting the size of the eddies which are responsible for the turbulent mixing process.

6.2 Operating condition and ambient flow effects

Operating condition and ambient flow effects in ABL flow on wake development are discussed. A distinction is made between effects on mean velocity distribution and turbulence distribution in the wake.

Mean velocity wake development

In contrast to the experiments in uniform flow the wake is rapidly mixed by the ambient turbulence. The measurements in ABL flow show, as in the uniform flow, a downshift of the wake. The downshift is in both experiments for $X \leq 5$ D of equal magnitude.

The wake is characterised by the maximum velocity defect ΔU_{max}. The velocity defect is caused by the drag of the turbine. When the turbine is operated at optimum power ($\lambda = 6.6$) the drag is $C_T = .74$, fig. 7.
At higher λ (8.5 and 9.3) the drag is high ($C_T = .81$ and .87) and velocity defects for $X \leq 2D$ are increased, fig. 27. For $X > 2D$ velocity defects are approximately equal at tip-speed ratios of $\lambda = 6.6$, 8.5 and 9.3.
At low λ (4.7 and 3.5) velocity defects decrease remarkable, according to low C_T.

Locations in which the velocity defect is $\frac{1}{2}\Delta U_{max}$ characterise the width of the wake. Inspection of table 5 shows an elliptical cross-section shape of the wake, in which horizontal dimensions are greater. This is probably caused by two related effects.
a. Limitation of vertical growth by the ground (ground effect),
b. Vertical mixing in the ABL is less than lateral mixing.

It is common practice to distinguish a region close to the rotor in which wake decay is governed by the rotor.
The velocity defect in this region is often approximated by:

$$\frac{\Delta U}{U} = 1 - \sqrt{1 - C_T}$$

The end of this region is called X near wake: X_{NW}.
Beyond this region wake decay is governed by ambient flow effects (the far wake).

Several definitions of X_{NW} are used.

a. The location ($X_{NW\ I}$) where the measured $\Delta U/U_r$ is equal to $1 - \sqrt{1 - C_T}$, see table 8.
b. For computation purposes the velocity decay in the far wake is approximated by:

$$\frac{\Delta U}{U} \sim (\frac{X}{D})^b$$

The location of intersection of the near wake approximation and far wake approximation is $X_{NW\ II}$.

In figure 28 the far wake is approximated by a least square error fit of measurements at X/D = 3, 4, 5, 6 and 7. $X_{NW\ II}$ is indicated by an asterix. Results are tabulated in table 8.

The near wake length is dependent on ambient flow radial turbulence intensities. In fig. 29 correlation of $X_{NW\ II}$ with v'/U of the rotor used is shown.

Turbulence in the wake

Close to the turbine, X = 2D, at off-centerline positions excesses in turbulence intensity are measured, fig. 30. This is probably caused by diminishing tip vortices. The turbulence intensity in the wake is dependent on tip-speed ratio. High tip-speed ratios generate high turbulence levels. This is illustrated by centerline turbulence intensities in fig. 31.

Vermeulen [6] correlates augmentation of wake turbulence (for $X > X_{NW\ II}$) above ambient levels with the drag of the rotor. Correlation in ABL flow is shown in fig. 32. Data originates from table 8.

7. CONCLUSIONS

Wind turbine tower effects are found only in the lower part of the wake.

Wind turbine nacelle effects are not found.

By describing the wake by a velocity defect profile superpositioned on an ambient flow profile the following conclusions are drawn.

Ground effects inhibit vertical growth of the lower part of the wake.

Turbine drag, dependant on operating conditions, and centerline velocity defects are strongly interrelated.

The velocity defect profile of a wind turbine shifts slightly towards the ground, by an angle of approximately 1 degree.

REFERENCES

[1] Vermeulen, P.E.J.,
A Wind Tunnel Study of the Wake of a Horizontal Axis Wind Turbine,
MT-TNO 78-09674, September 1978.

[2] Builtjes, P.J.H., Vermeulen P.E.J.,
Atmospheric Boundary Layer Simulation in the PIA and MIA Wind tunnels of TNO-Apeldoorn,
MT-TNO 80-290, January 1980.

[3] Vermeulen, P.E.J.,
Studies of the Wake Structure of Model Wind Turbine Generators,
MT-TNO 79-012904, November 1979.

[4] Vermeulen, P.E.J.,
Invloed van oppervlakteruwheid en turbulentie op de statische drukverdeling rond cirkelcylinders bij hoge Reynoldsgetallen (in Dutch),
MT-TNO 78-08357, 1978.

[5] ESDU Wind Engineering Vol. 1a 74031.

[6] Alfredson, P.H., Dahlberg, J.A.,
A preliminary Wind Tunnel Study of Windmill Wake Dispersion in Various Flow Conditions,
FFA-TN-AU-1499 part 7, 1979.

[8] Clayton, B.R., Filby, P.
Wind Turbine Wake Studies,
proc. 3rd BWEA Wind Energy Conference, Cranfield 1981.

[9] Talmon, A.M.,
Windtunnelonderzoek naar invloeden van toren en gondel op het zog van een windturbine,
MT-TNO 84-08479, 1984.

Table 1 Drag of the towers

Tower	A (m^2)	C_T tower
cylindrical	$8.8\ 10^{-3}$	1.16
lattice	$22.1\ 10^{-3}$	0.38

Table 2 Characteristic locations of the wake in uniform flow

X/D	model configuration	location of ΔU_{max}	vertical profile location of $\frac{1}{2}\Delta U_{max}$		horizontal halfwidth *
			lower side	upper side	
2	●	-0.11 (Z/D)	-0.59 (Z/D)	0.44 (Z/D)	0.47 (Y/D)
2	□	-0.11	-0.58	0.44	0.48
2	o	-0.03	-0.58	0.44	0.48
2	✱	-0.06	-0.56	0.45	0.48
5	●	-0.20	-0.65	0.35	0.46
5	□	-	-0.64	0.33	-
5	o	-0.14	-0.61	0.37	0.47
5	✱	-0.14	-0.63	0.35	0.47
9.6	●	-0.31	< -0.83	0.24	0.46
9.6	□	-0.31	< -0.83	0.23	0.45
9.6	o	-0.25	0.71	0.25	0.45
9.6	✱	-0.25	0.70	0.23	0.47

* mean of locations of $\frac{1}{2}\Delta U_{max}$ of right and left side.

Table 3 Properties of simulated ABL flow

coordinates (Z = 0 ground)			U (z) [m/s]	u' [m/s]	w' [m/s]	x_{Lu} [m]	x_{Lw} [m]	sample freq. (Hz)	measuring period (s)
X	Y	Z							
0	0	0.60	10.50	1.11	.89	.82	.32	65	2 x 30
0	0	0.35	9.92	1.15	.87	.88	.34	65	2 x 30
0	0	0.35	9.62	1.25	.86	.92	.32	200	2 x 10
0	0	0.10	8.68	1.32	.62	.91	.20	65	2 x 30
					v' [m/s]		x_{Lv} [m]		
0	0	.35	9.48	1.14	1.21	.76	.47	65	2 x 30

Table 4 Wake traverses in ABL flow

λ	X/D	vertical traverse coordinates	horizontal traverse coordinates
4.5	2	Y = 0	Z/D = -0.08
4.5	4	= 0	= -0.13
4.5	7	= 0	= -0.14
6.6	2	Y = 0	Z/D = -0.08
6.6	4	= 0	= -0.13
6.6	7	= 0	= -0.14
8.5	2	Y = 0	Z/D = -0.08
8.5	4	= 0	= -0.13
8.5	7	= 0	= -0.14

Table 5 Location of characteristic velocity defect locations

λ	X/D	$\Delta\bar{U}_{max}/\bar{U}_r$ vert. def. prof.	$\frac{Z}{D}(\Delta\bar{U}_{max})$	$\frac{Z}{D}(\frac{1}{2}\Delta\bar{U}_{max})$ upper side	$\frac{Z}{D}(\frac{1}{2}\Delta\bar{U}_{max})$ lower side	$\Delta\bar{U}_{max}/\bar{U}_r$ hor.def. prof.	$\frac{Y}{D}(\frac{1}{2}\Delta\bar{U}_{max})$
4.5	2	.390	-0.08	0.36	-0.56	.395	0.47
	4	.215	-0.13	0.39	-0.64	.225	0.65
	7	.125	-0.14	0.47	-0.71	.105	0.81
6.6	2	.545	-0.08	0.33	-0.50	.535	0.49
	4	.245	-0.13	0.40	-0.65	.255	0.63
	7	.120	-0.14	0.52	-0.76	.120	0.81
8.5	2	.605	-0.08	0.39	-0.51	.610	0.51
	4	.240	-0.13	0.46	-0.71	.255	0.65
	7	.110	-0.14	0.47	-0.75	.115	0.88

Table 6 Centerline velocity defect decay

X/D	$\lambda = 3.5$ $\Delta\bar{U}_{max}/\bar{U}_r$	$\lambda = 4.5$ $\Delta\bar{U}_{max}/\bar{U}_r$	$\lambda = 6.6$ $\Delta\bar{U}_{max}/\bar{U}_r$	$\lambda = 8.5$ $\Delta\bar{U}_{max}/\bar{U}_r$	$\lambda = 9.3$ $\Delta\bar{U}_{max}/\bar{U}_r$
1	.36	.48	.64	.79	.82
2	.27	.38	.51	.59	.58
3	.21	.28	.35	.35	.35
4	.14	.21	.24	.24	.23
5	.13	.17	.18	.16	.16
6	.092	.13	.14	.15	.13
7	.087	.091	.093	.10	.11

Table 7 Turbulence intensities at characteristic locations

λ	X/D	centerline	vertical traverse				horizontal traverse			
			upper side		lower side		right		left	
		u'/U_r	Z/D	u'/U_r	Z/D	u'/U_r	Y/D	u'/U_r	Y/D	u'/U_r
4.5	2	.14	.4	.21	-.4	.14	.4	.20	-.4	.17
4.5	4	.15	"	.17	"	.13	"	.17	"	.15
4.5	7	.13	"	.14	"	.13	"	.15	"	.13
6.6	2	.17	"	.23	"	.16	"	.24	"	.20
6.6	4	.17	"	.18	"	.15	"	.19	"	.17
6.6	7	.15	"	.14	"	.14	"	.14	"	.14
8.5	2	.20	"	.24	"	.20	"	.24	"	.24
8.5	4	.18	"	.18	"	.16	"	.18	"	.18
8.5	7	.14	"	.14	"	.13	"	.14	"	.14

Table 8 Description of wake centerline

λ	C_T	$X_{NW\ I}/D$ according to $1\sqrt{1-C_T}$ *1	Description of far wake $\frac{\Delta U_{max}}{U_r} = a\left(\frac{X}{D}\right)^b$ *2 a	b	$X_{NW\ II}/D$ according to intersection of lines *3	Turbulence at centerline $\frac{\Delta u'}{U_r} C_T\ [10^{-3}]$ *4 $\frac{X}{D}$: 2	3	4	5	6	7
9.2	0.87	1.7	1.57	-1.39	1.91	93	97	86	50	41	19
8.5	0.81	2.0	1.66	-1.41	2.15	99	104	74	53	32	23
6.6	0.74	2.1	1.89	-1.50	2.46	65	95	69	51	38	38
4.5	0.54	2.4	1.20	-1.27	2.82	49	64	65	49	42	22
3.5	0.42	2.4	0.64	-1.04	2.58	43	52	57	64	48	29

*1 use is made of fig. 27

*2 least square error method for X/D > 2

*3 see fig. 30

*4 $\frac{\Delta u'}{U_r}$ is calculated as: $\frac{u'(x,0,0) - u'_r(x, -1.67\ D, 0)}{U_r\ (X, -1.67\ D, 0)}$

Model configurations.

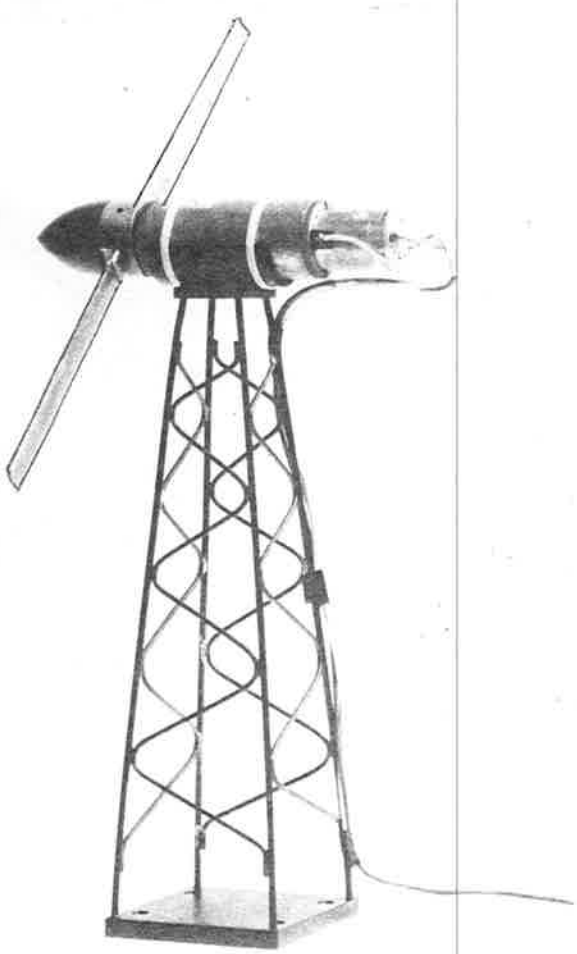

lattice tower,
cylindrical nacelle

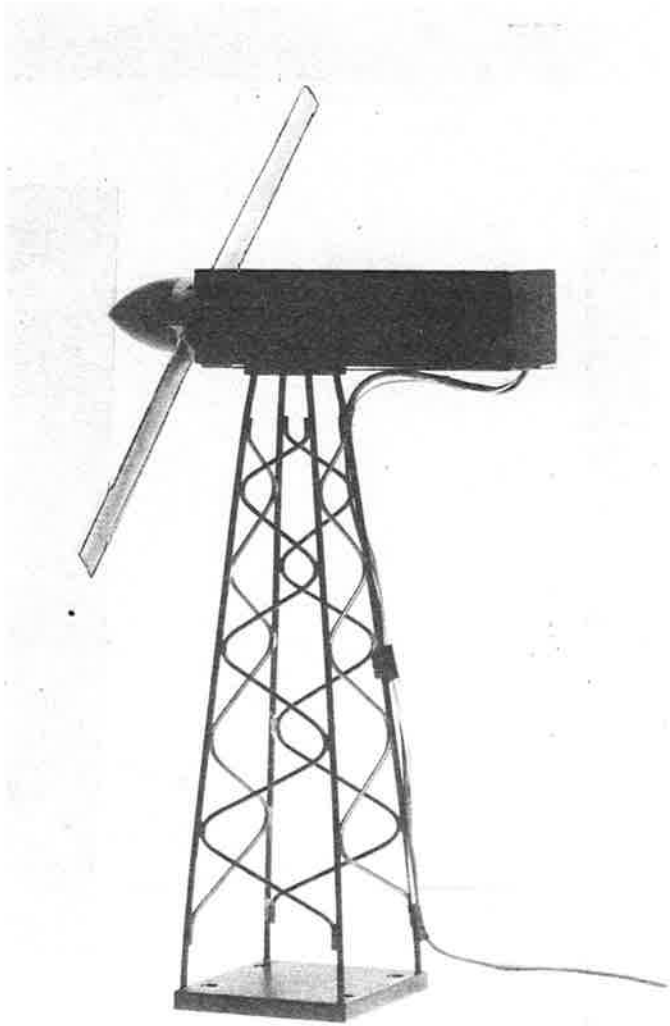

lattice tower,
rectangular nacelle

MT-TNO
12433
Fig. 1b

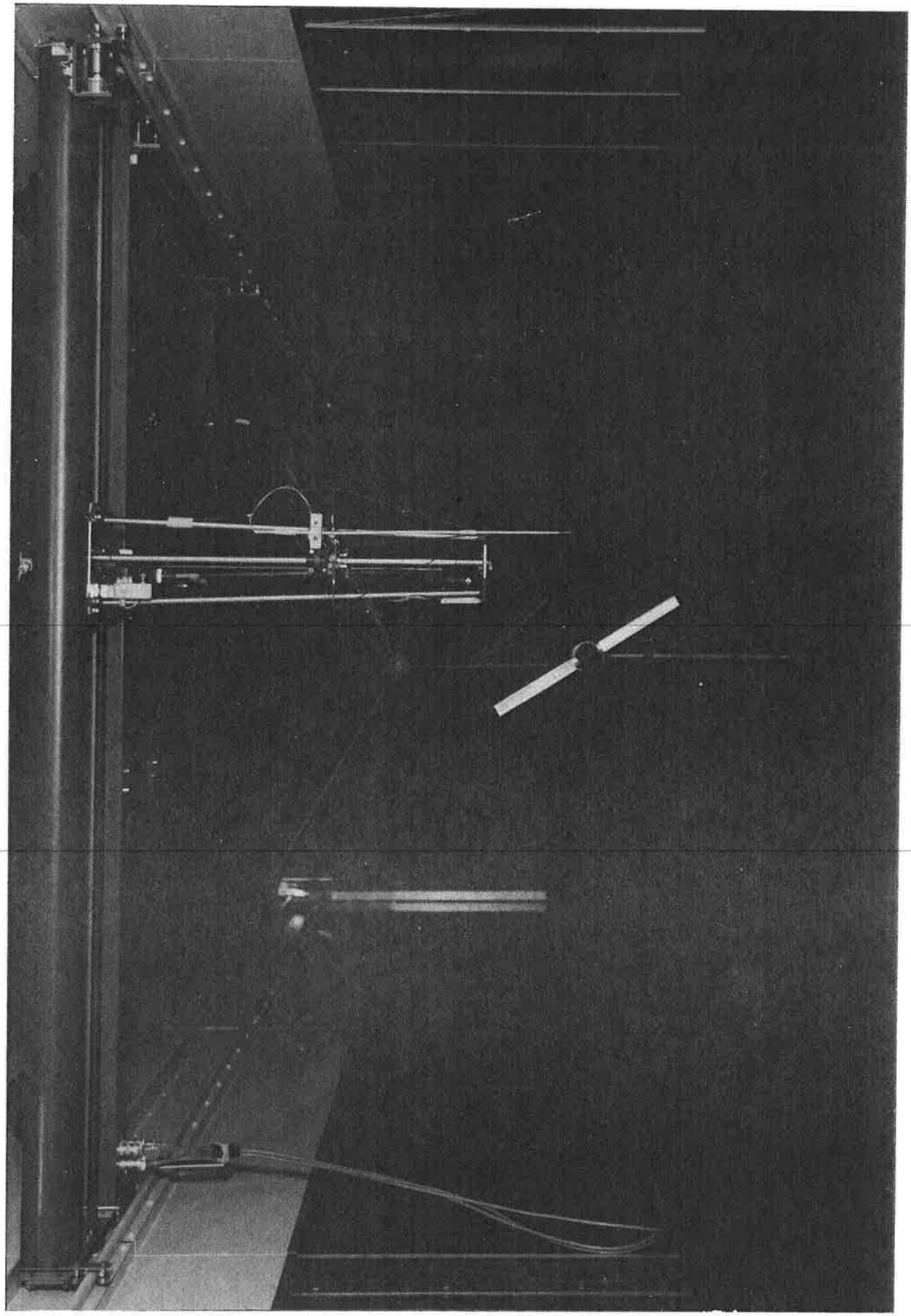

The windturbine in the ABL flow experiments, downstream view.

MT_TNO
12433
Fig. 2a

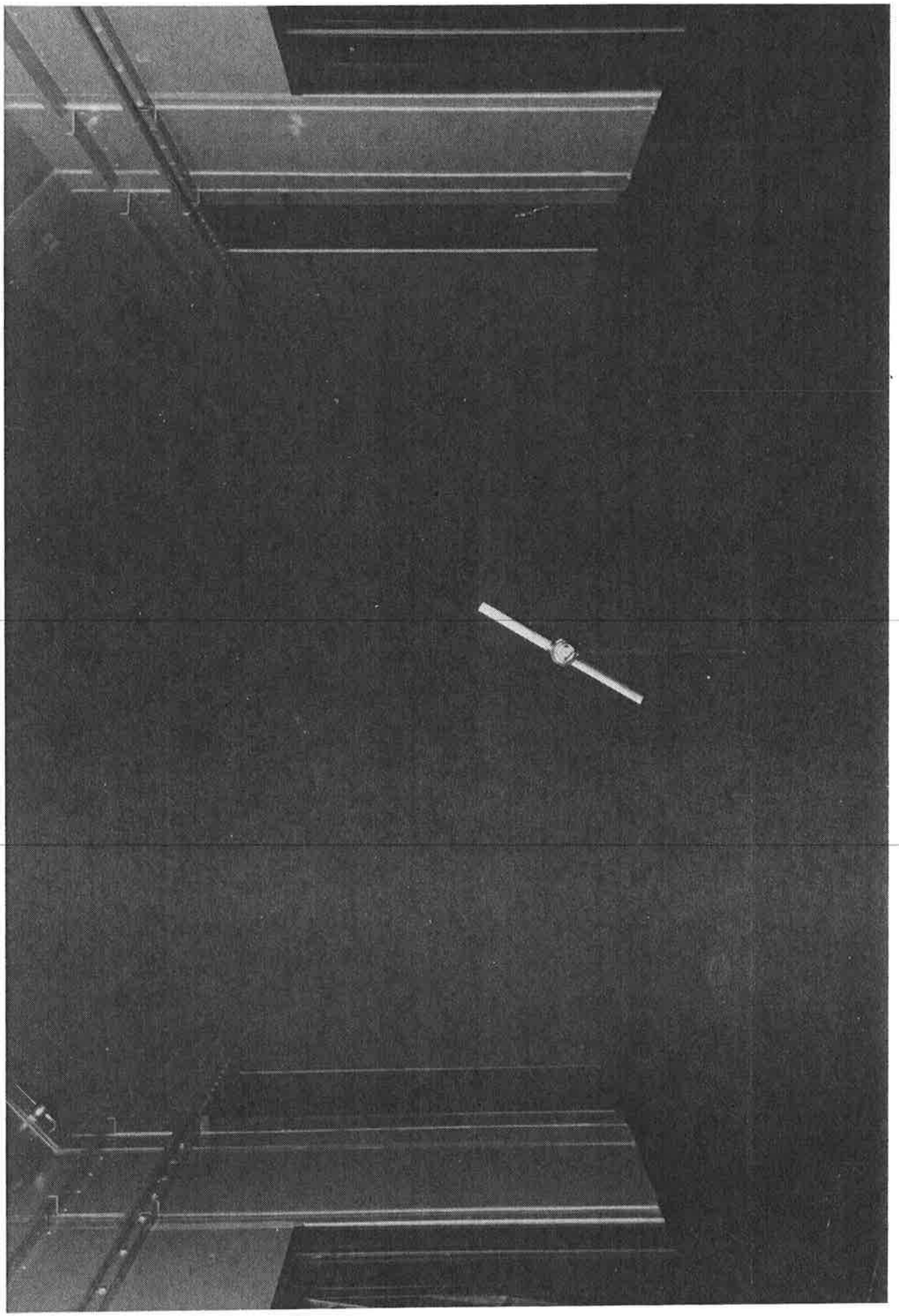

The windturbine in the ABL flow experiments, upstream view.

MT_TNO
12433
Fig. 2b

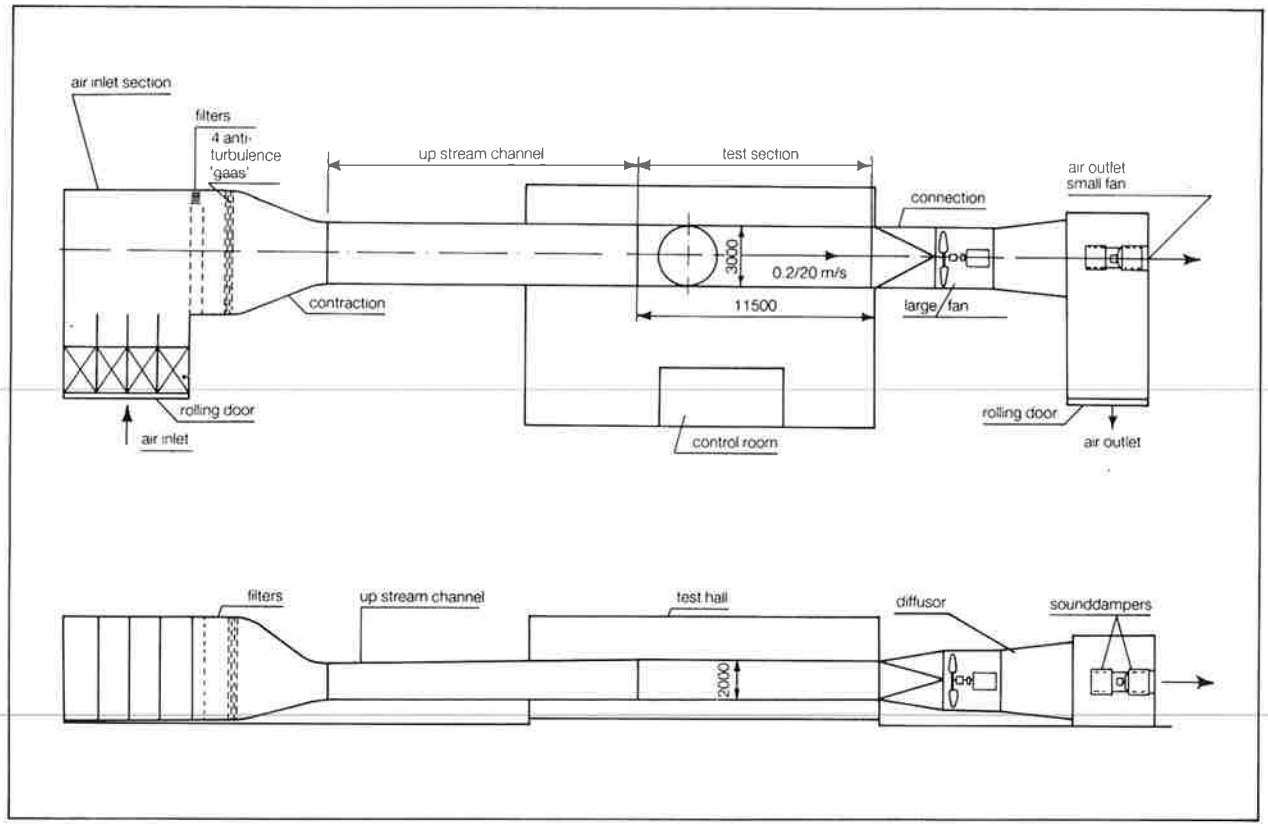

Windtunnel IV

The windtunnel used in the ABL flow measurements.

MT_TNO
12433
Fig.3

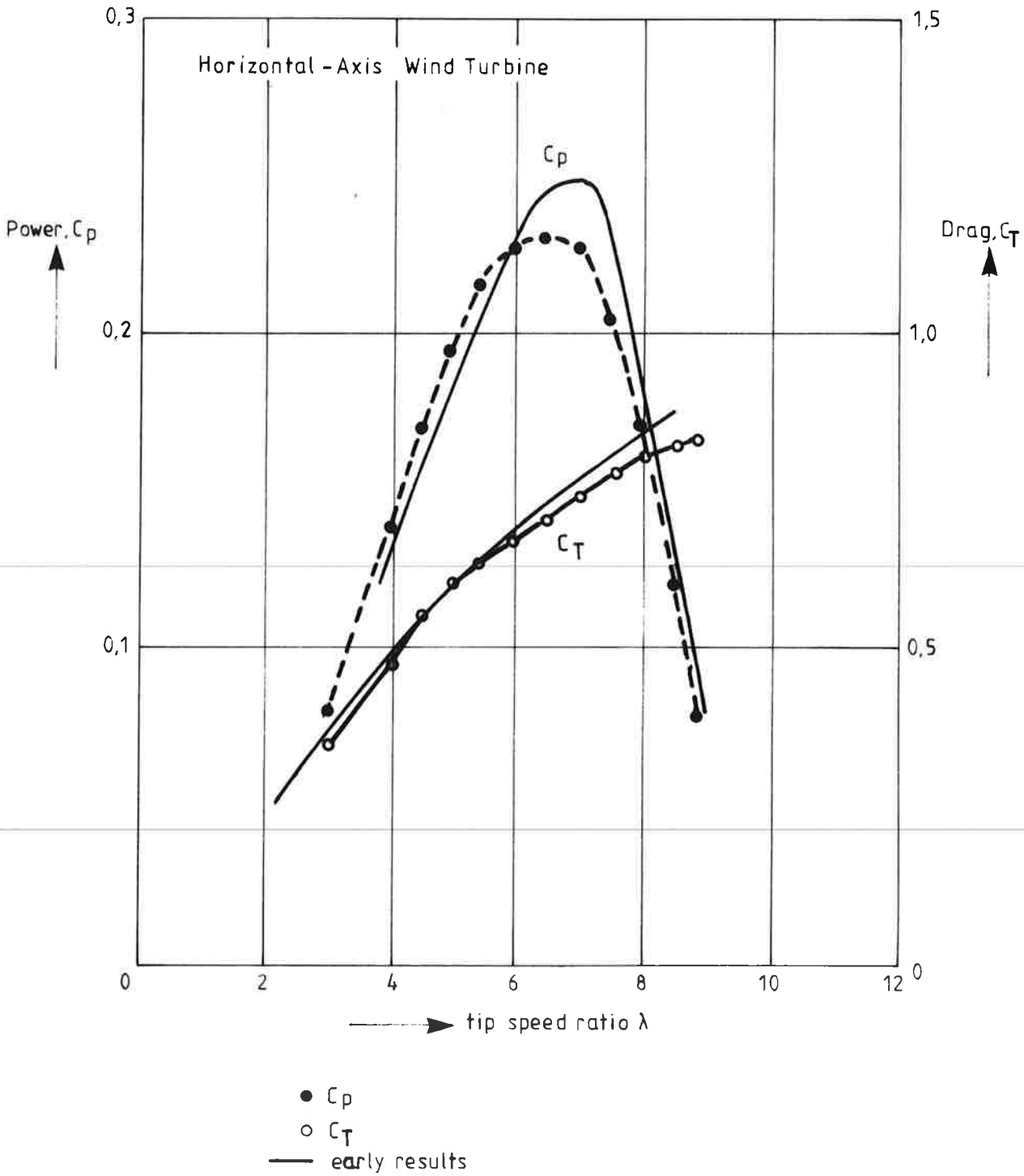

Power and Drag of the horizontal axis machine as a function of the tip-speed ratio at Ur = 8,6 m/s in uniform flow.

MT_TNO
12433
Fig. 4

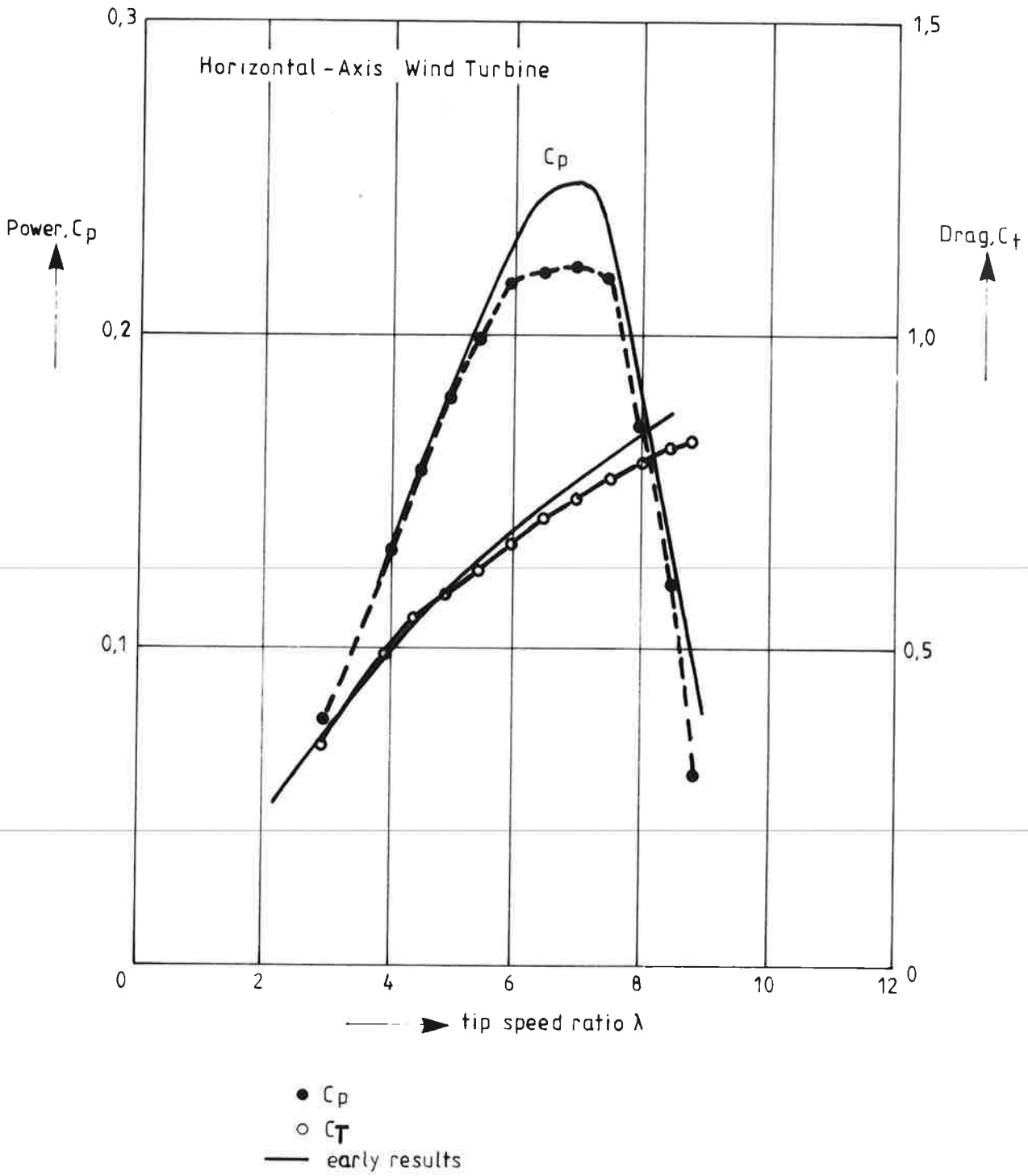

Power and Drag of the horizontal axis machine as a function of the tip-speed ratio at Ur = 9,7 m/s in uniform flow.

MT_TNO
12433
Fig.5

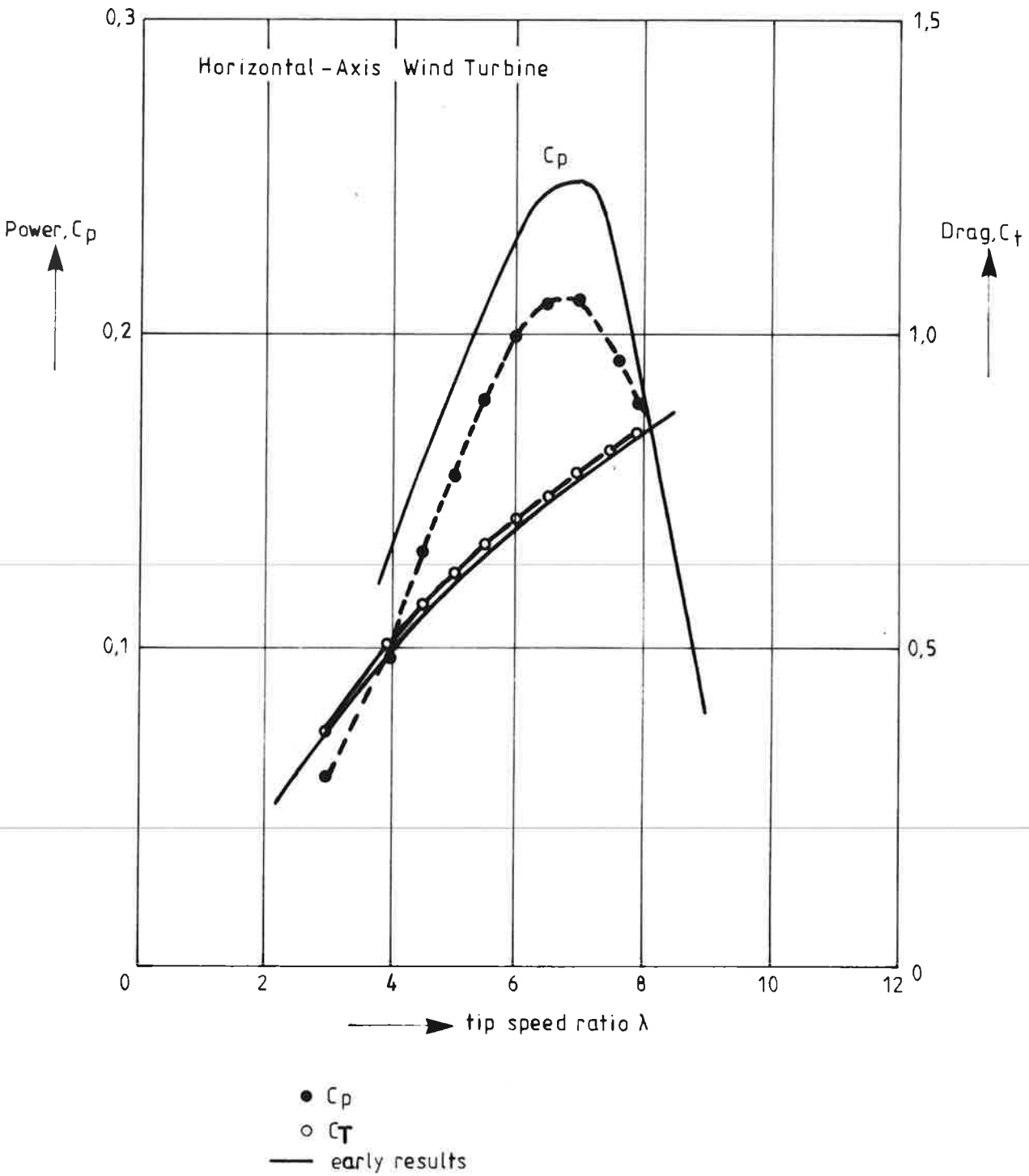

Power and Drag of the horizontal axis machine as a function of the tip-speed ratio at Ur=11,8m/s in uniform flow.

MT_TNO
12433
Fig.6

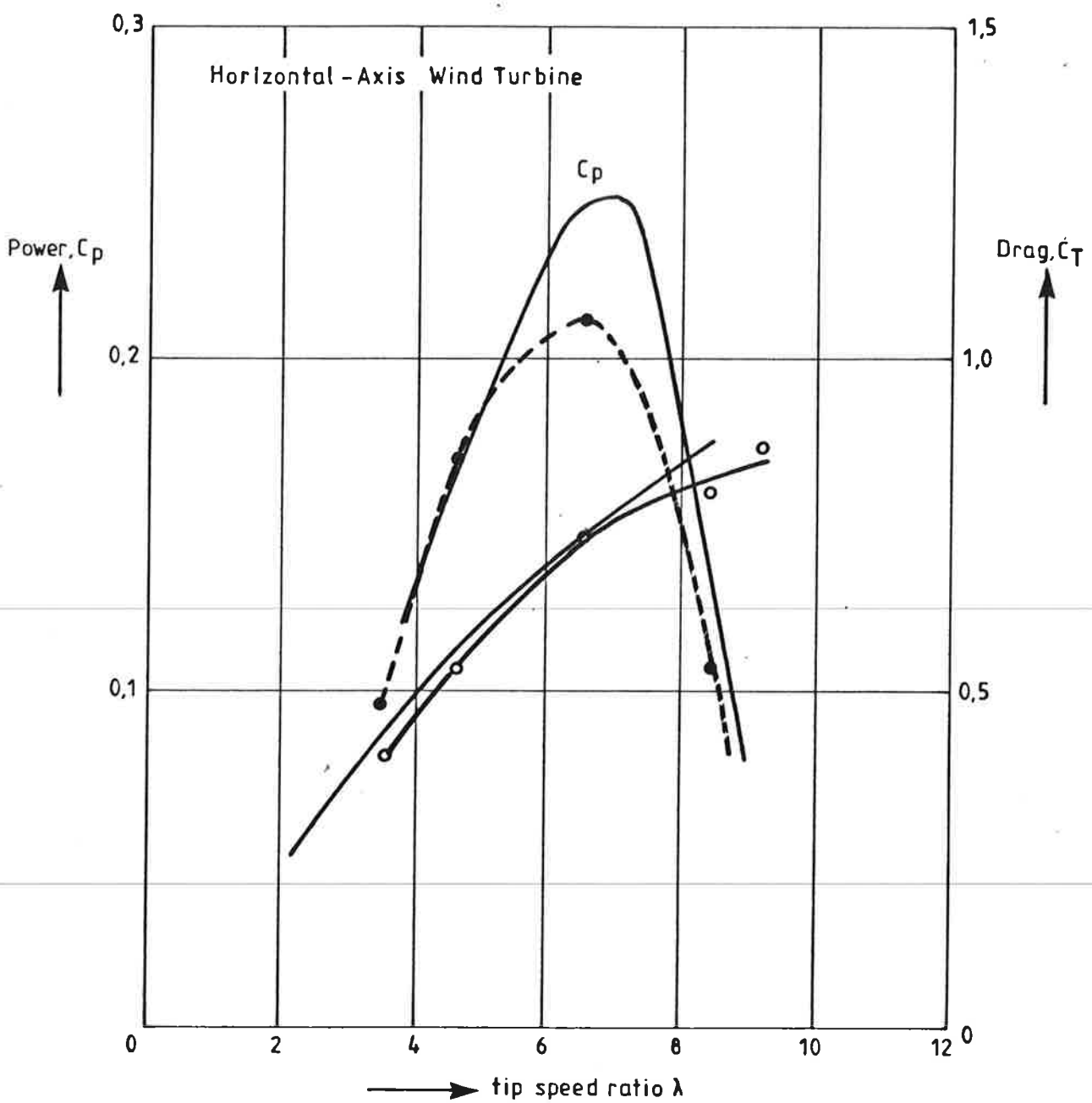

λ	C_p	C_t
3,5	0,099	0,42
4,7	0,165	0,55
6,6	0,213	0,74
8,5	0,111	0,81
9,3	–	0,87

Power and Drag of the horizontal axis machine as a function of the tip-speed ratio in ABL flow.

MT_TNO
12433
Fig. 7

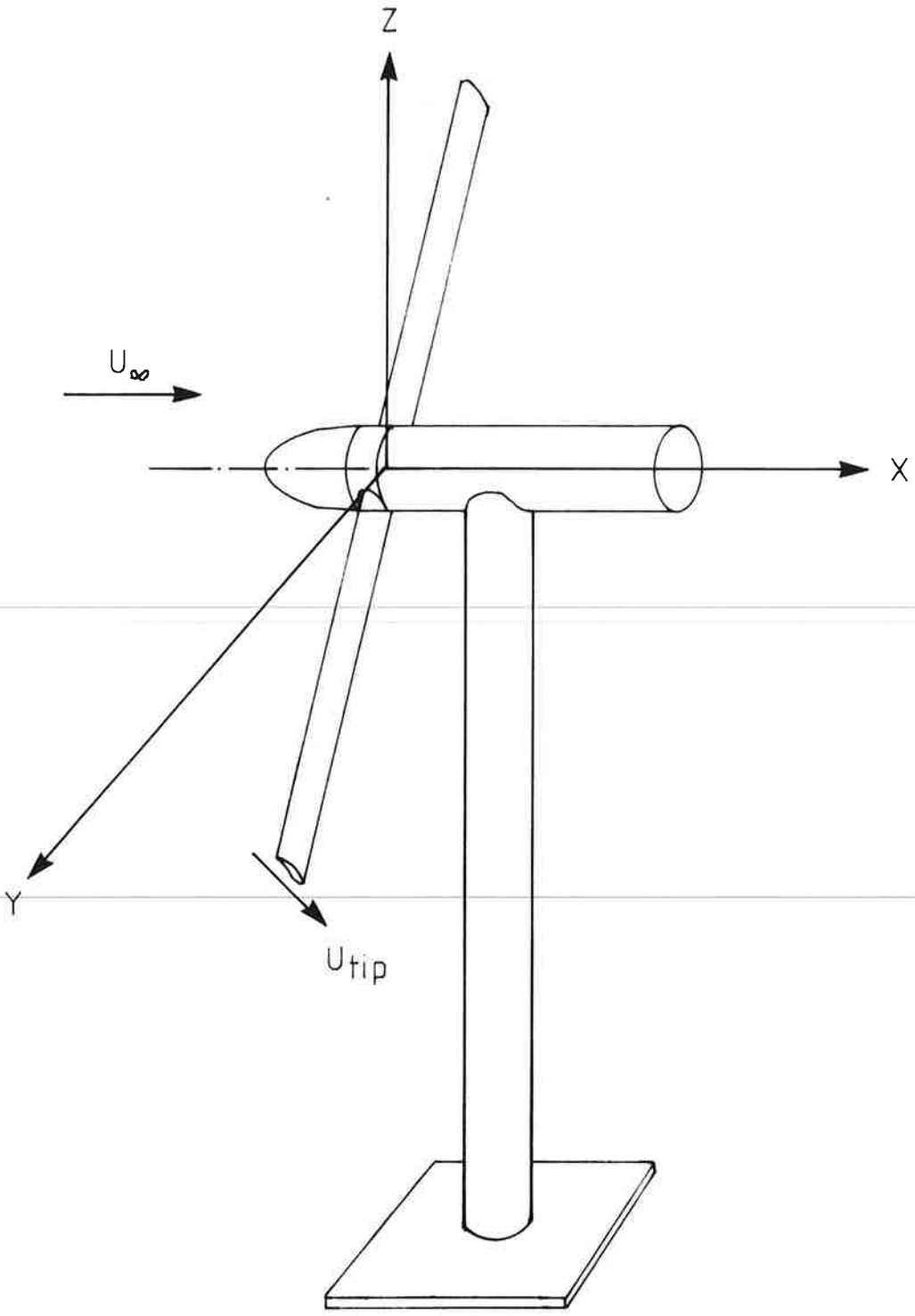

The coördinate system.

MT_TNO
12433
Fig. 8

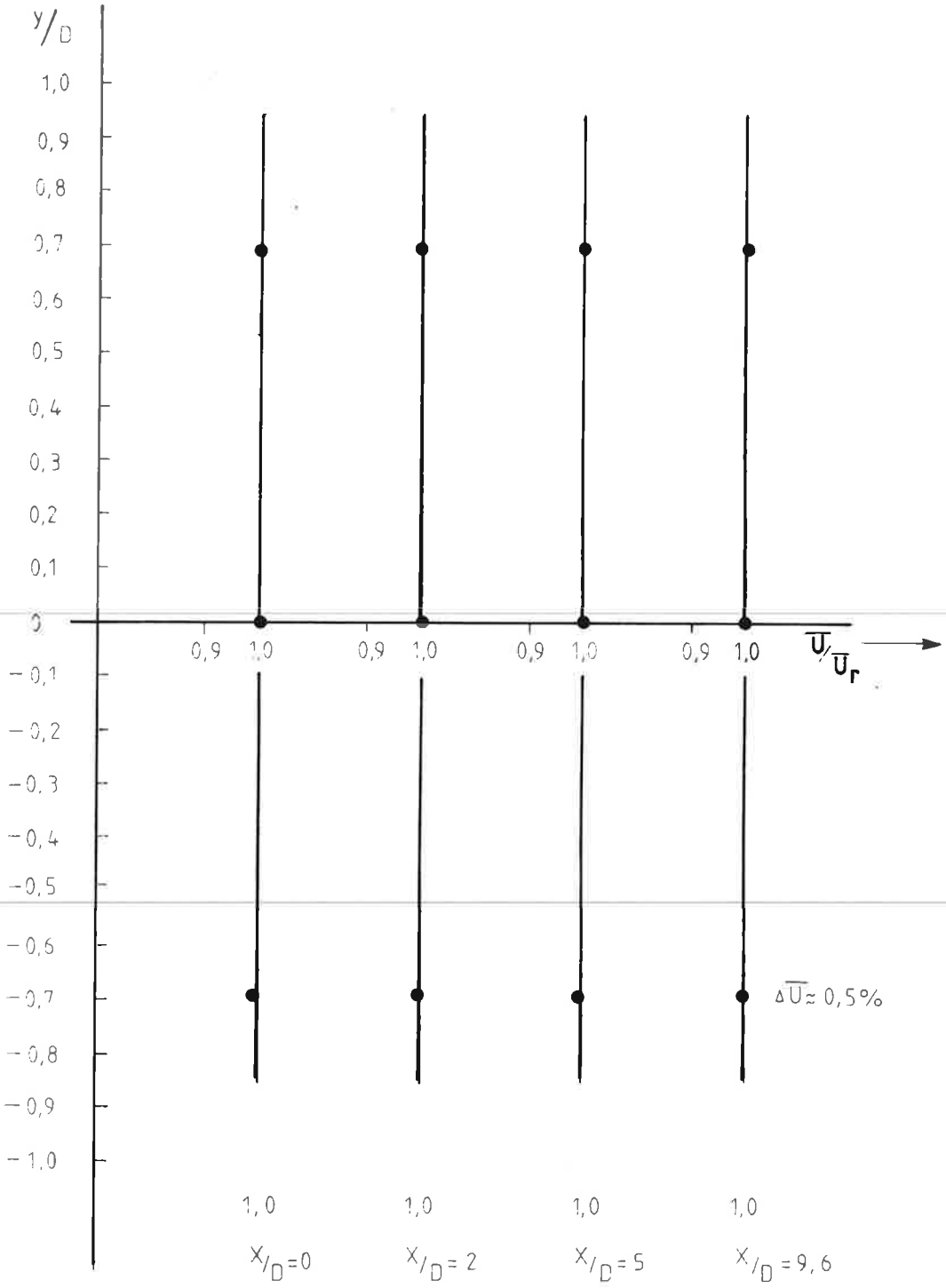

Horizontal profiles in uniform flow (at hub-height)

MT_TNO
12433
Fig. 9

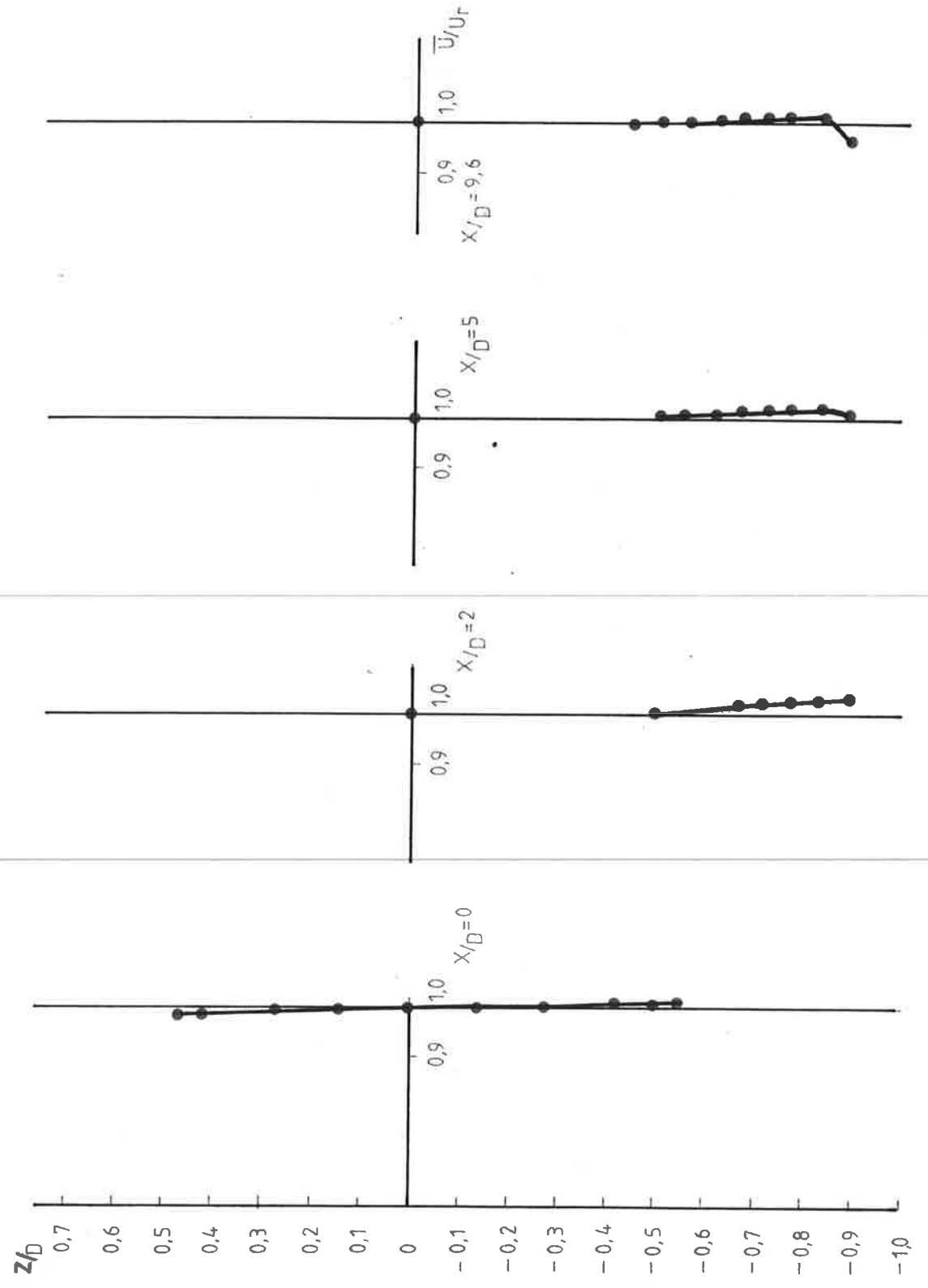

Vertical velocity profiles in uniform flow.

MT_TNO
12433
Fig. 10

Wake of the towers

MT_TNO
12433
Fig. 11

Vertical wake profiles.

MT_TNO
12433
Fig. 12

Characteristic vertical wake locations.

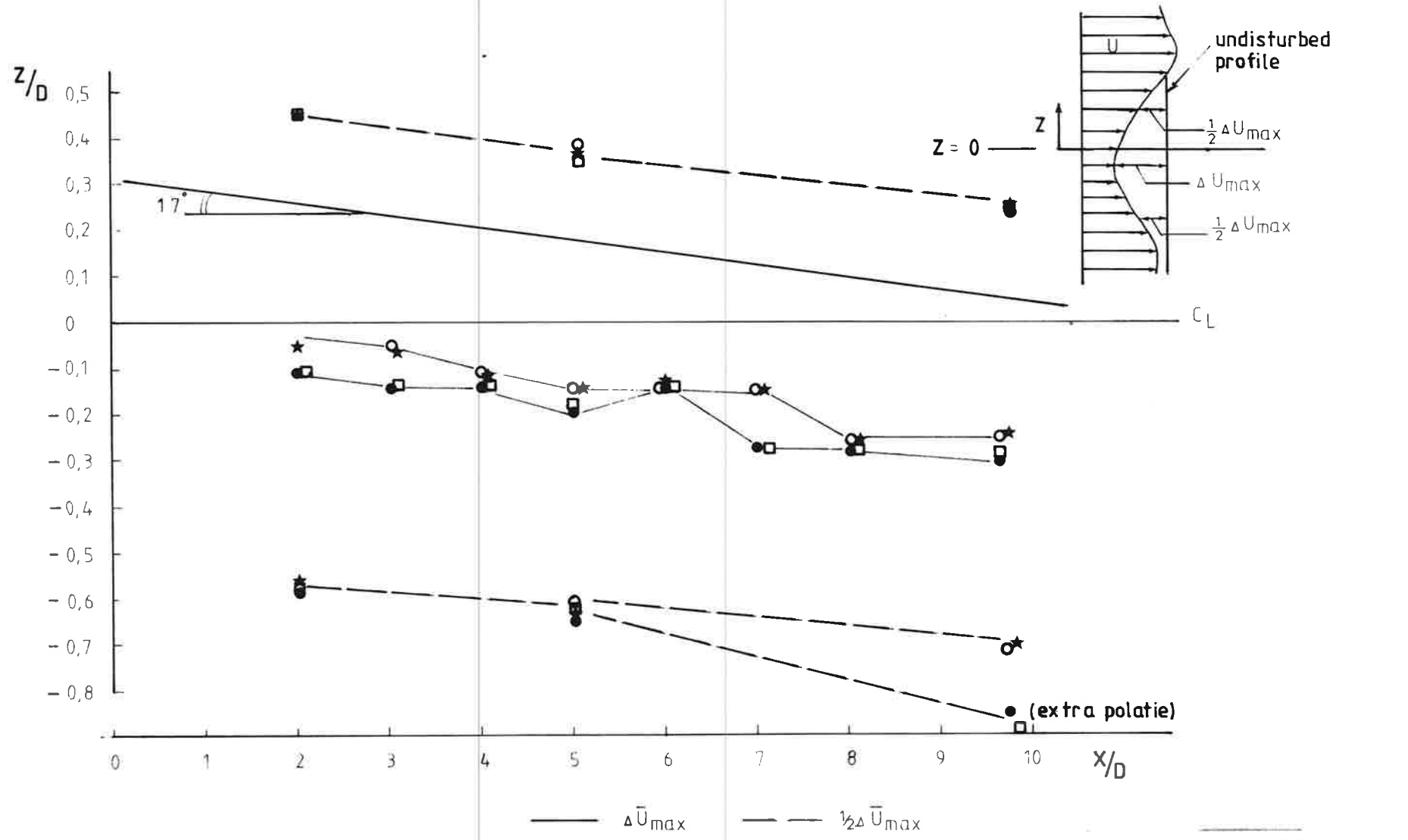

MT-TNO
12433
Fig. 13

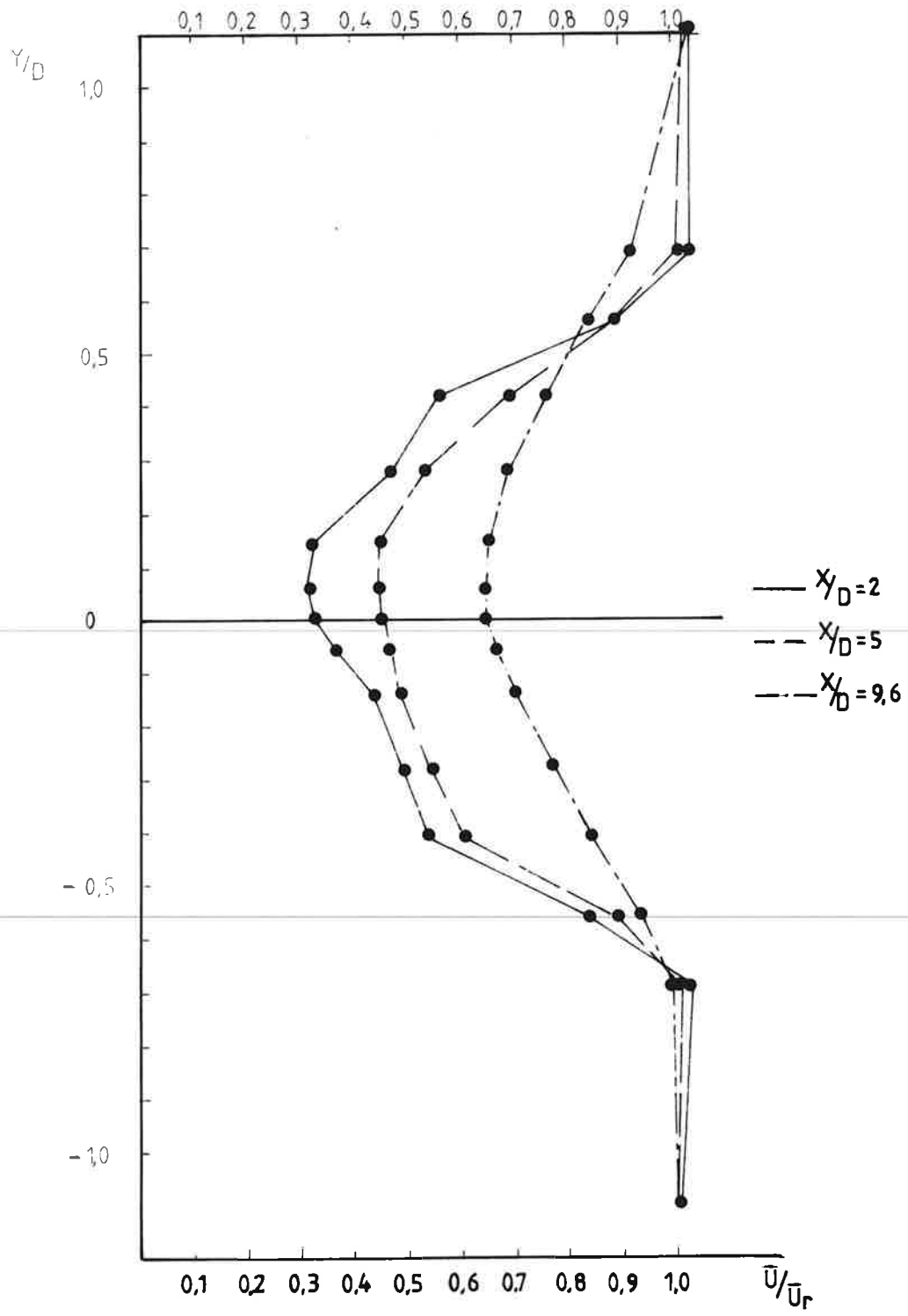

- ● cylindrical tower, cylindrical nacelle
- □ " " , rectangular "
- ○ lattice " , cylindrical "
- ★ " " , rectangular "

Wake decay.

MT_TNO
12433
Fig.14

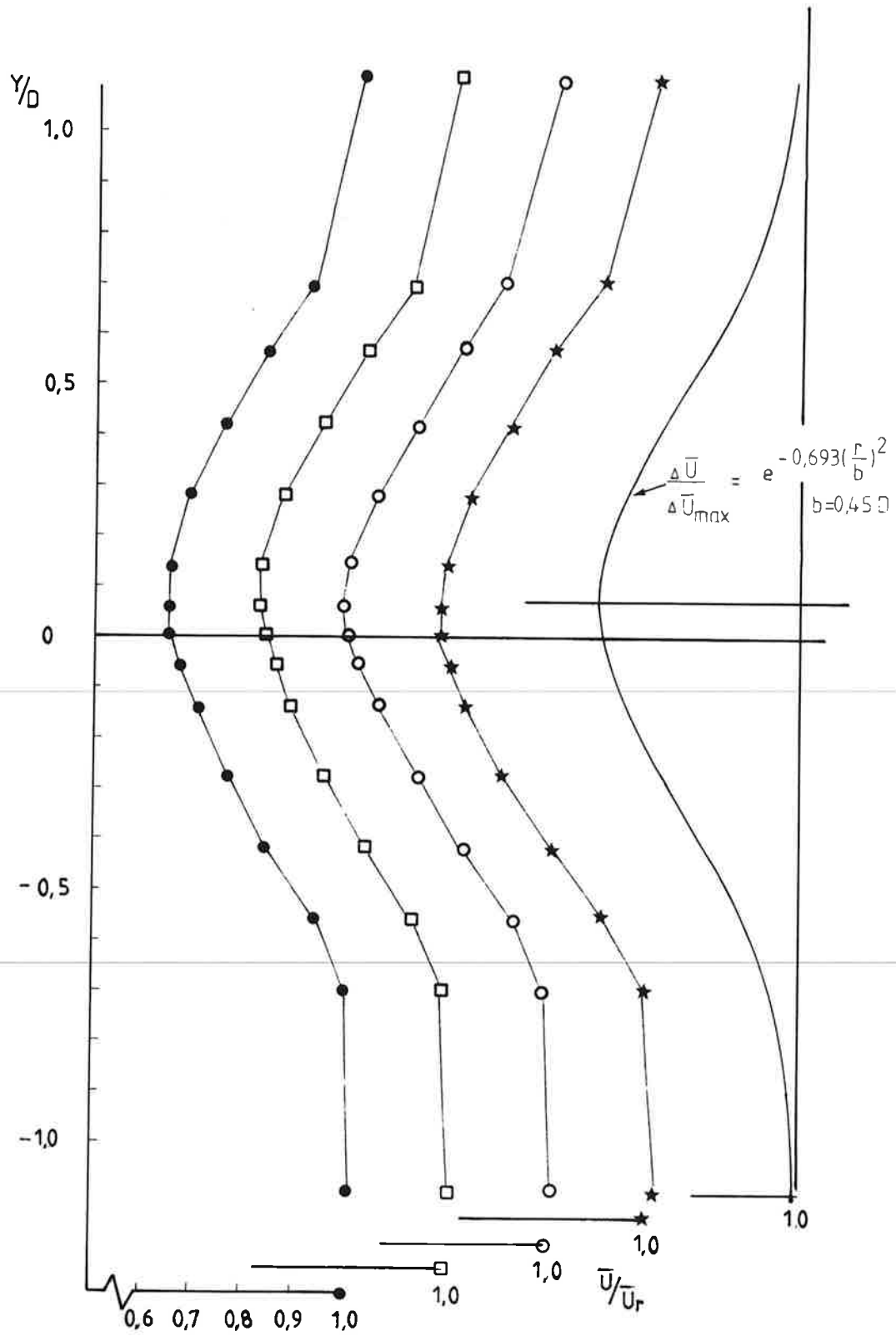

Horizontal profiles at X/D = 9,6, at Z-height of maximum velocity defect.

MT_TNO
12433
Fig. 15

Characteristic horizontal wake locations.

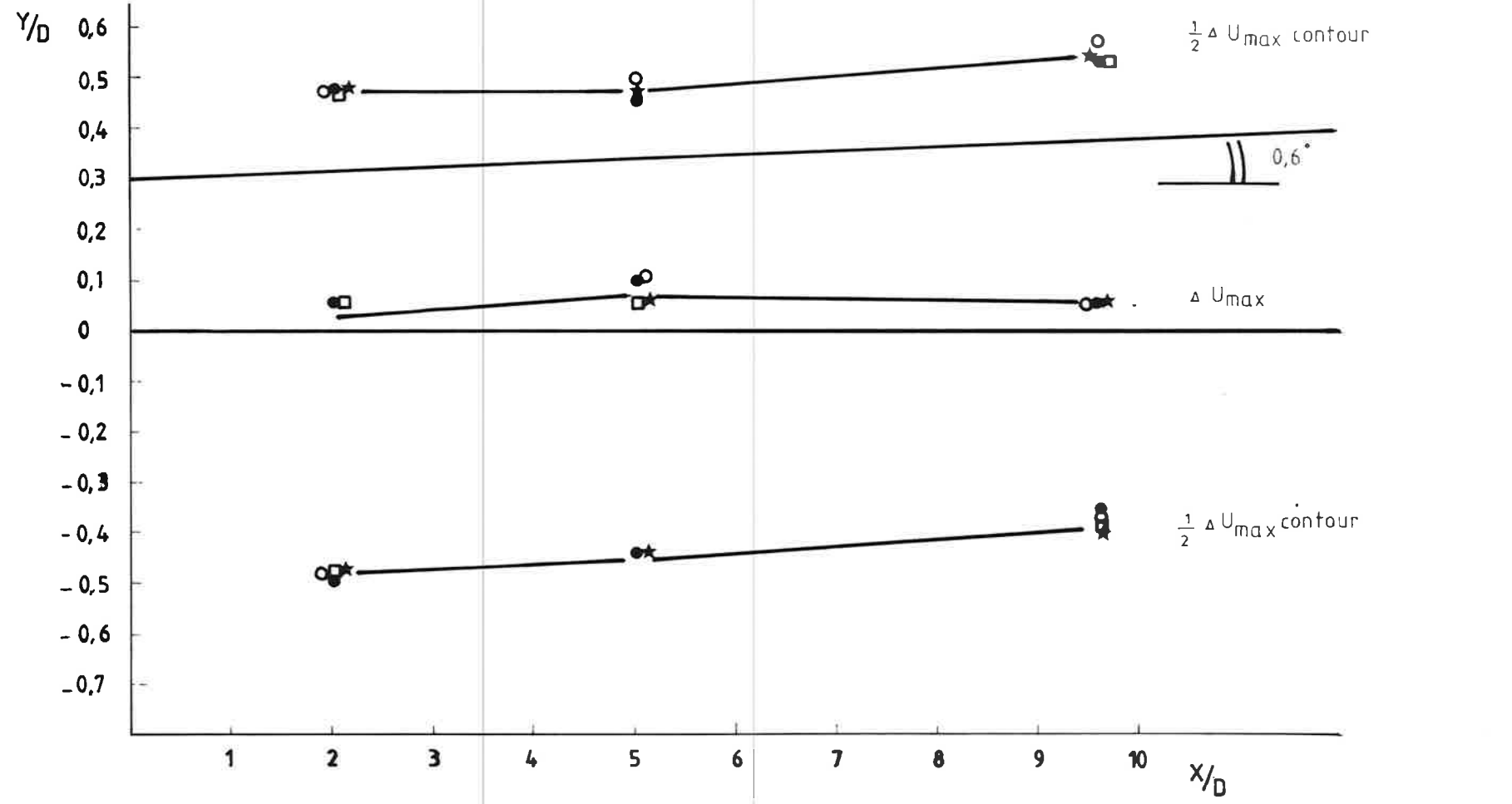

MT_TNO
12433
Fig. 16

Centerline velocity defect decay.

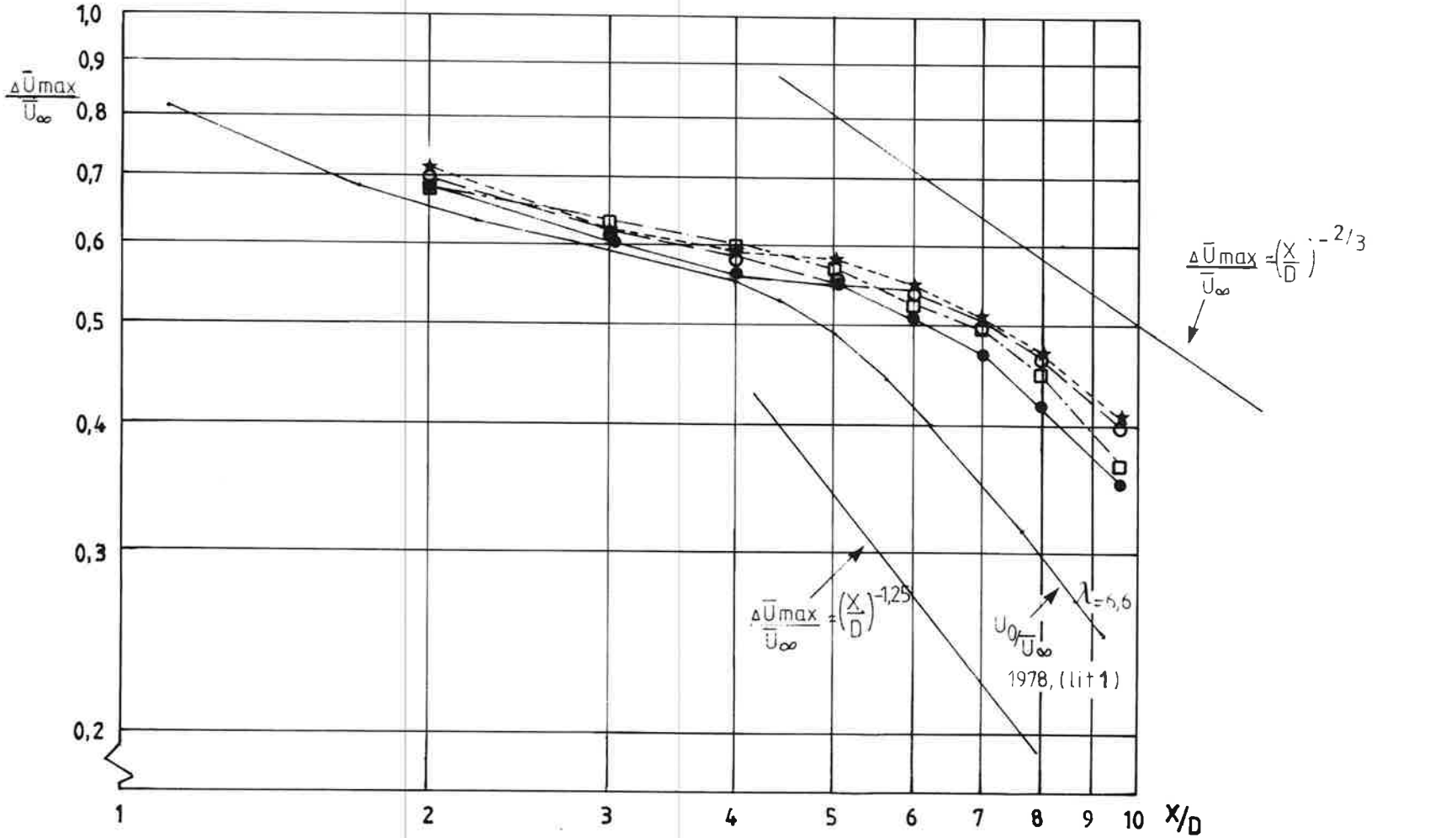

MT_TNO
12433
Fig. 17

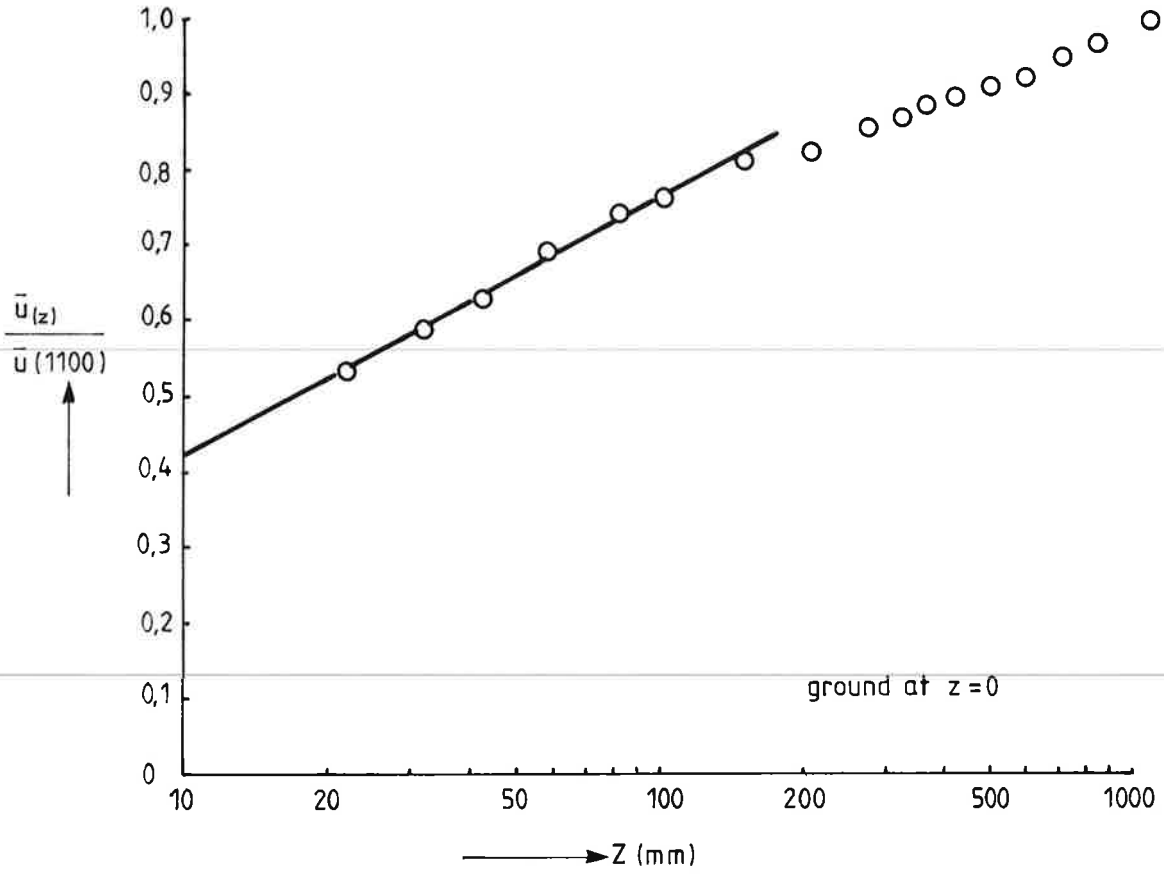

The vertical velocity profile in the ABL flow at x=0 y=0

MT_TNO
12433
Fig.18

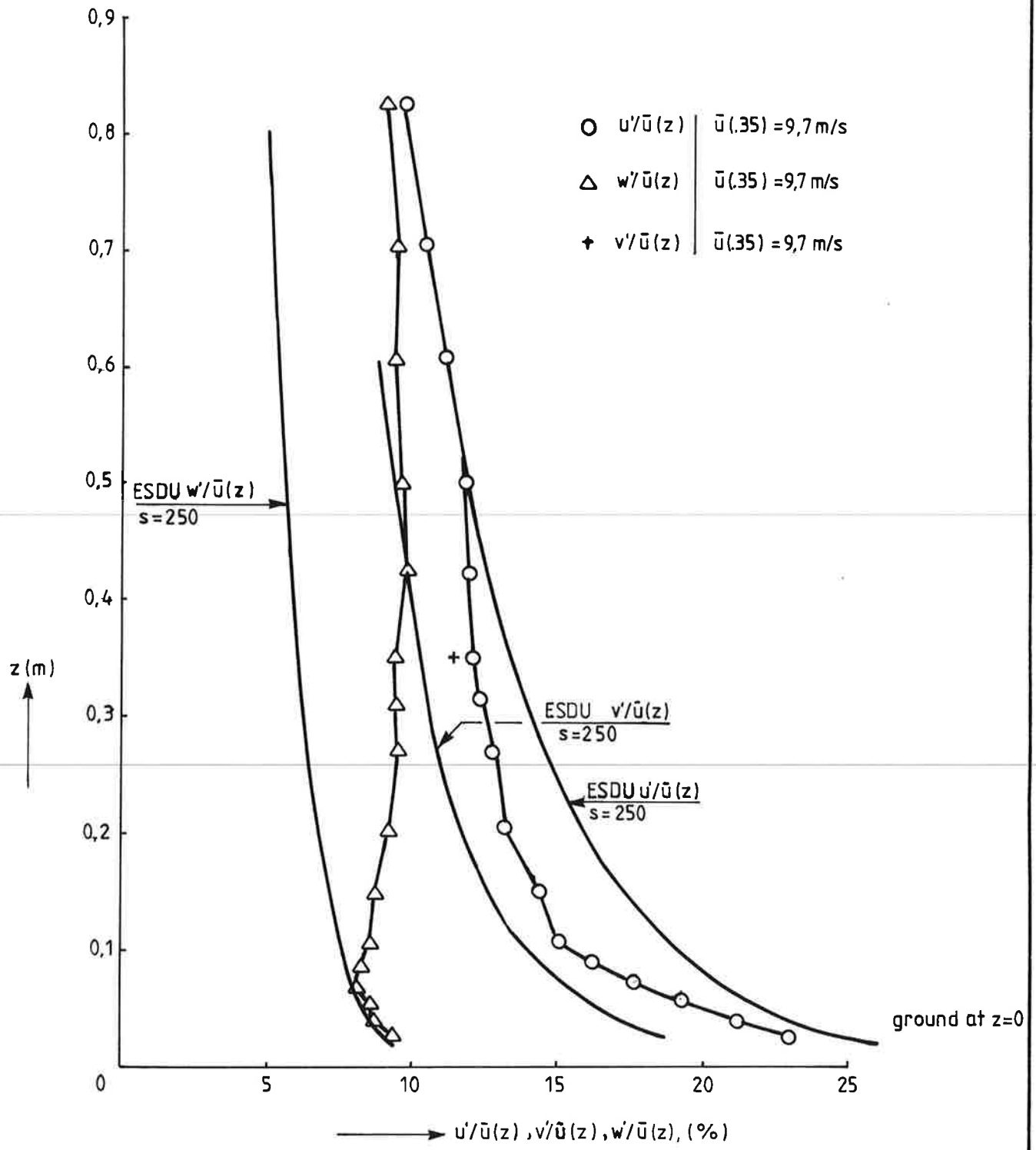

Turbulence intensities in the ABL flow

MT_TNO
12433
Fig.19

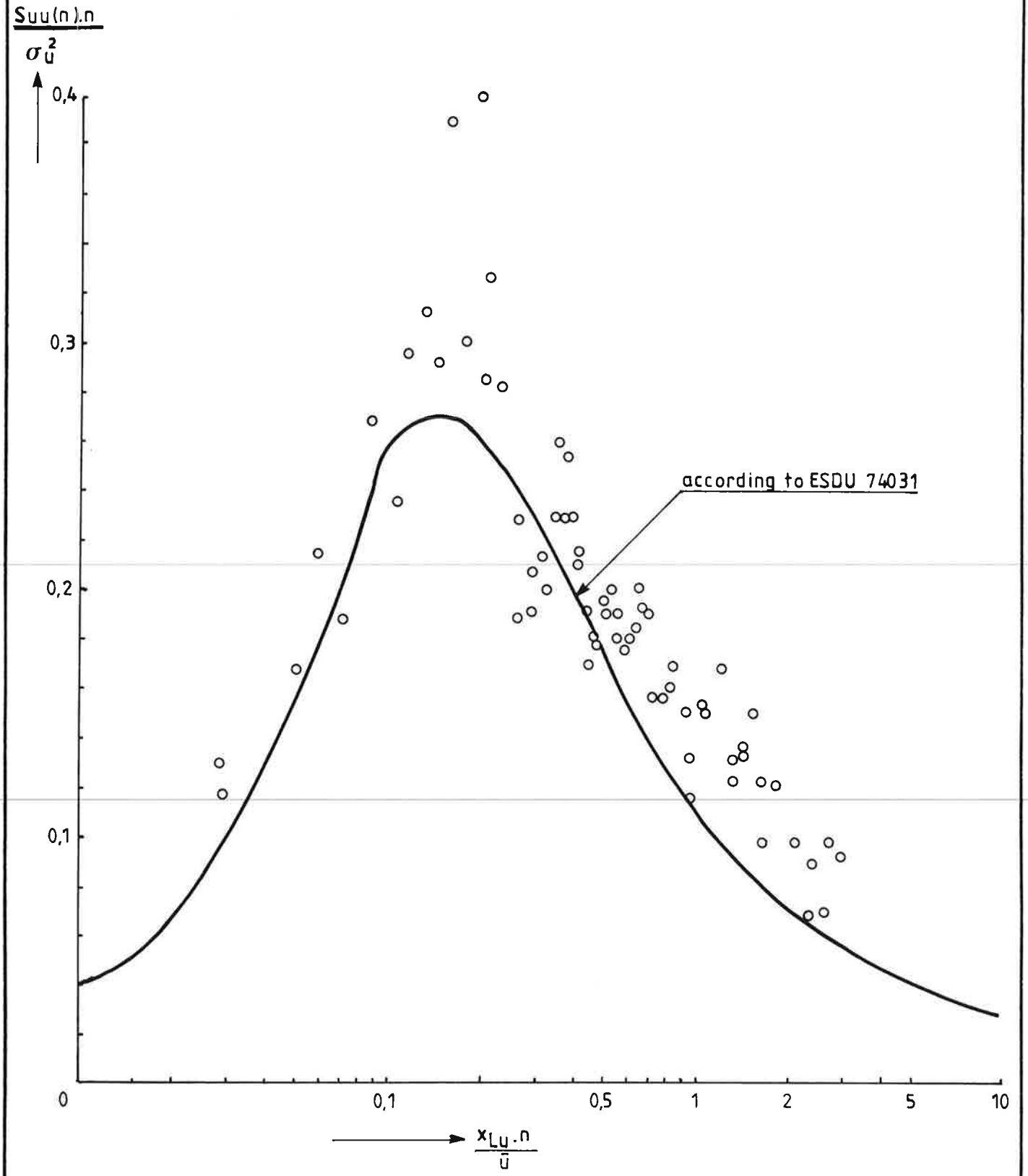

The power spectrum at „hub-height"

MT_TNO
12433
Fig. 20

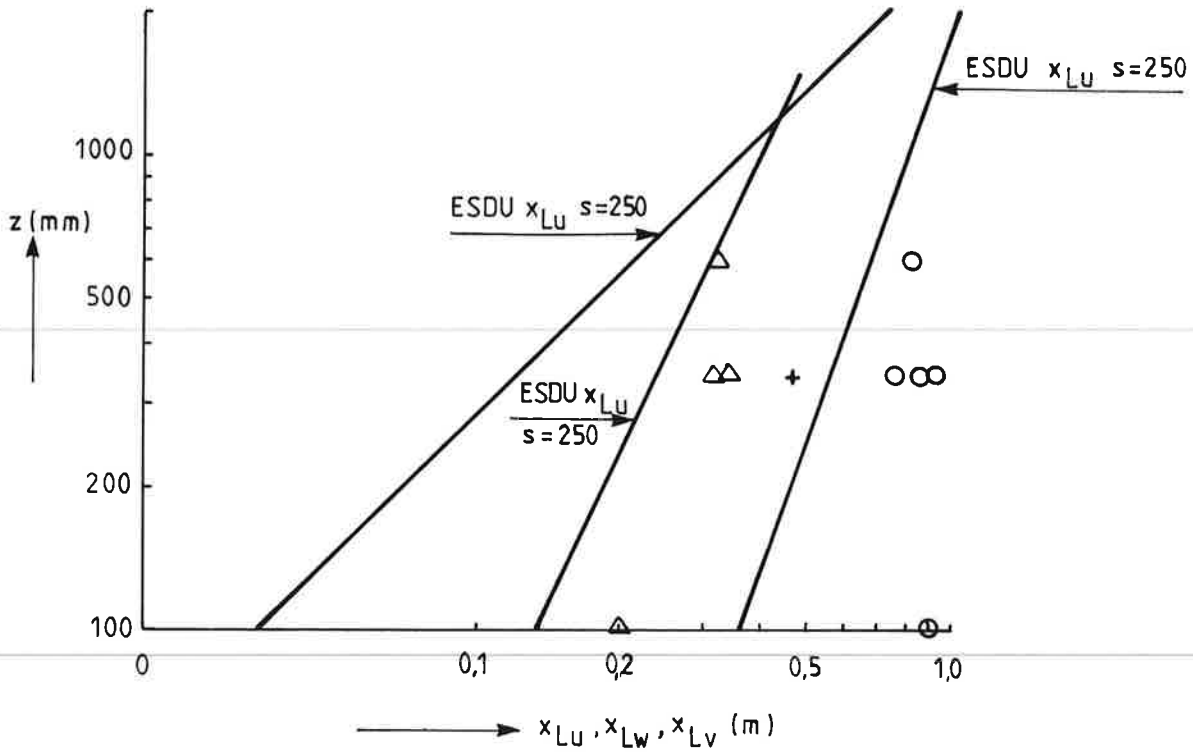

ground at z=0 , ○ = x_{Lu} , △ = x_{Lw} , + = x_{Lv}.

Integral lenght scales, comparison with ESDU 74031 at a scale of 1 : 250 and $z_o = 0{,}6.10^{-3}$ m

MT_TNO
12433
Fig.21

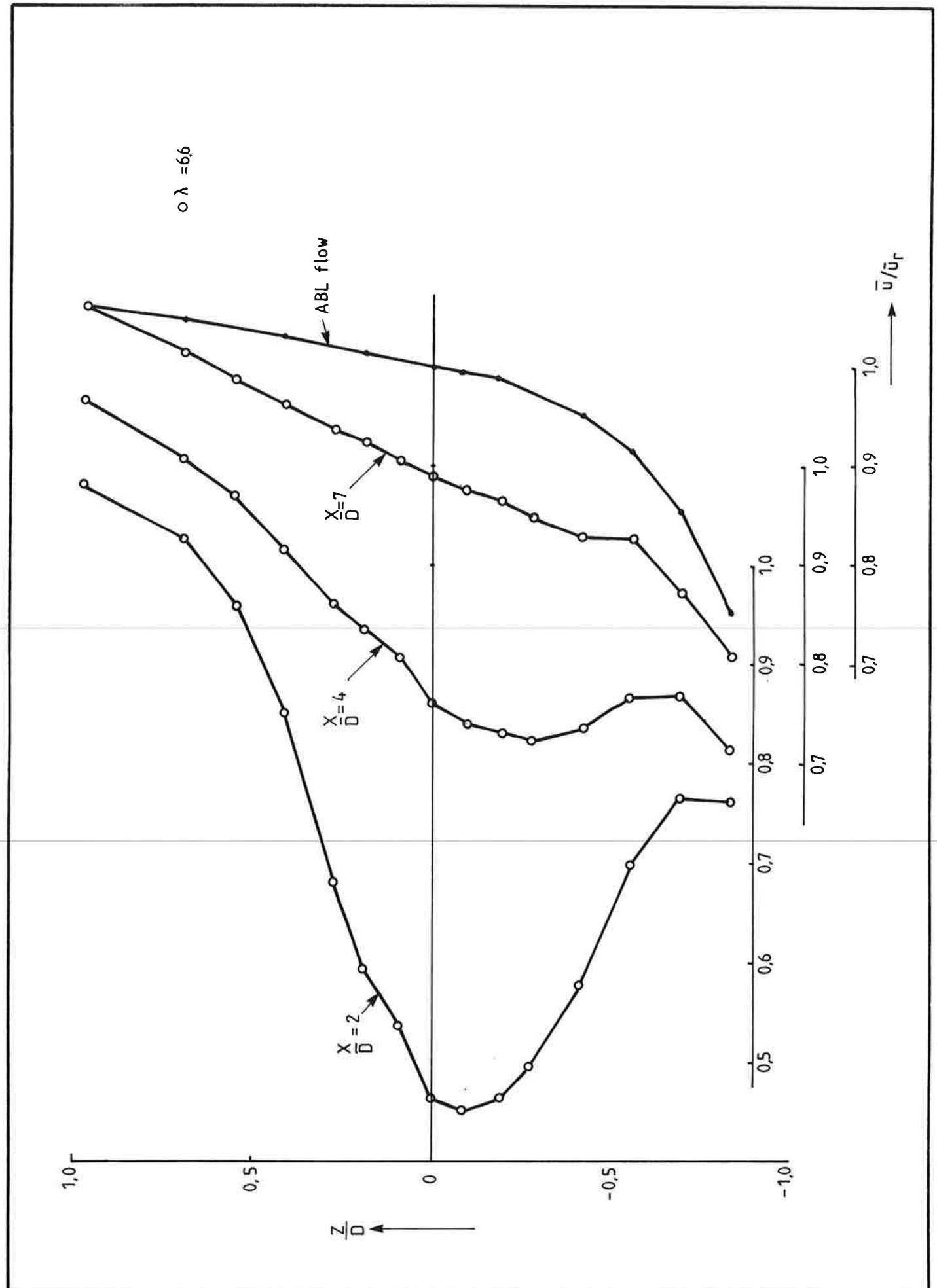

Vertical wake profiles at λ=6,6

MT_TNO
12433
Fig. 22

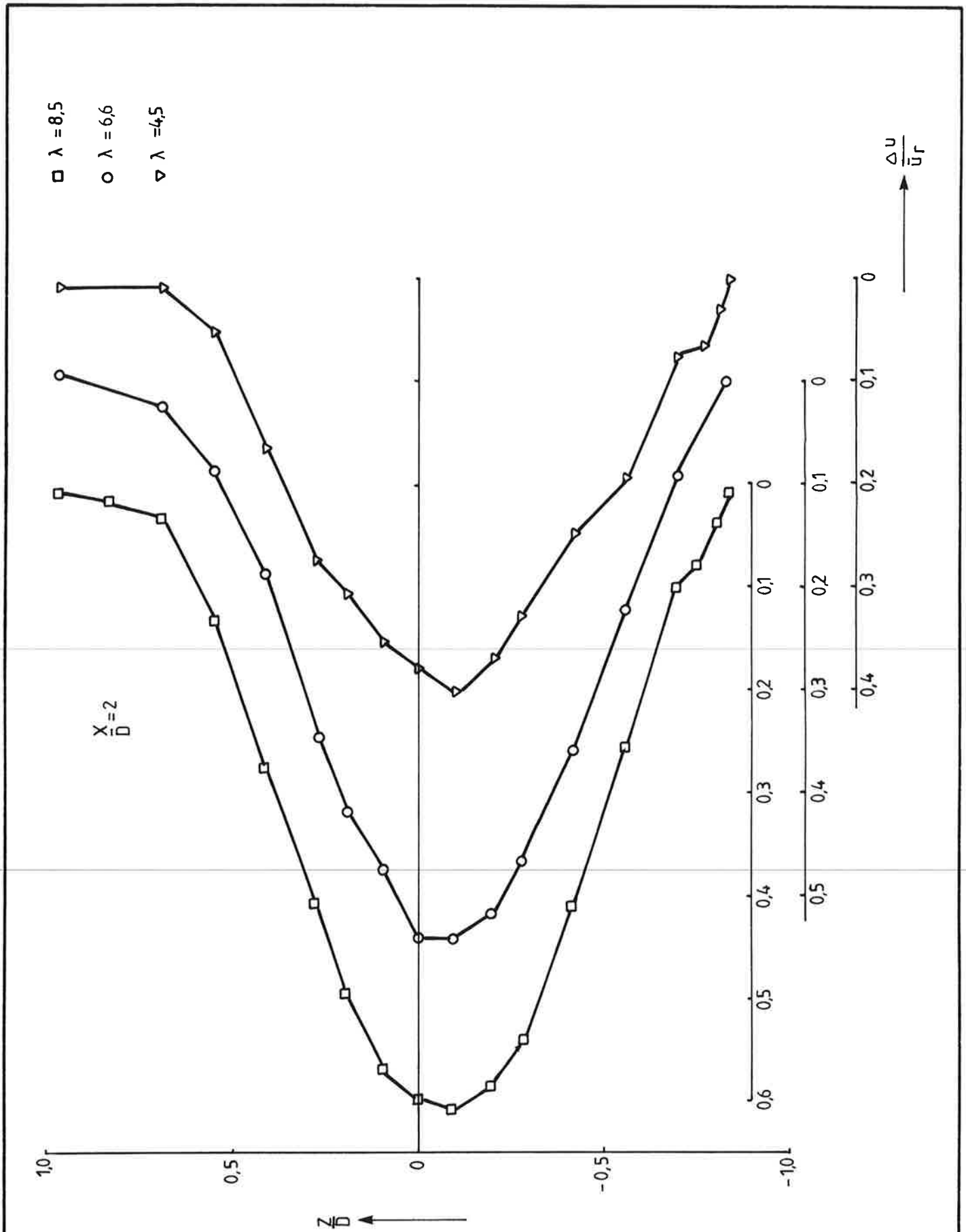

Vertical velocity defect profiles at X/D = 2

MT_TNO
12433
Fig. 23

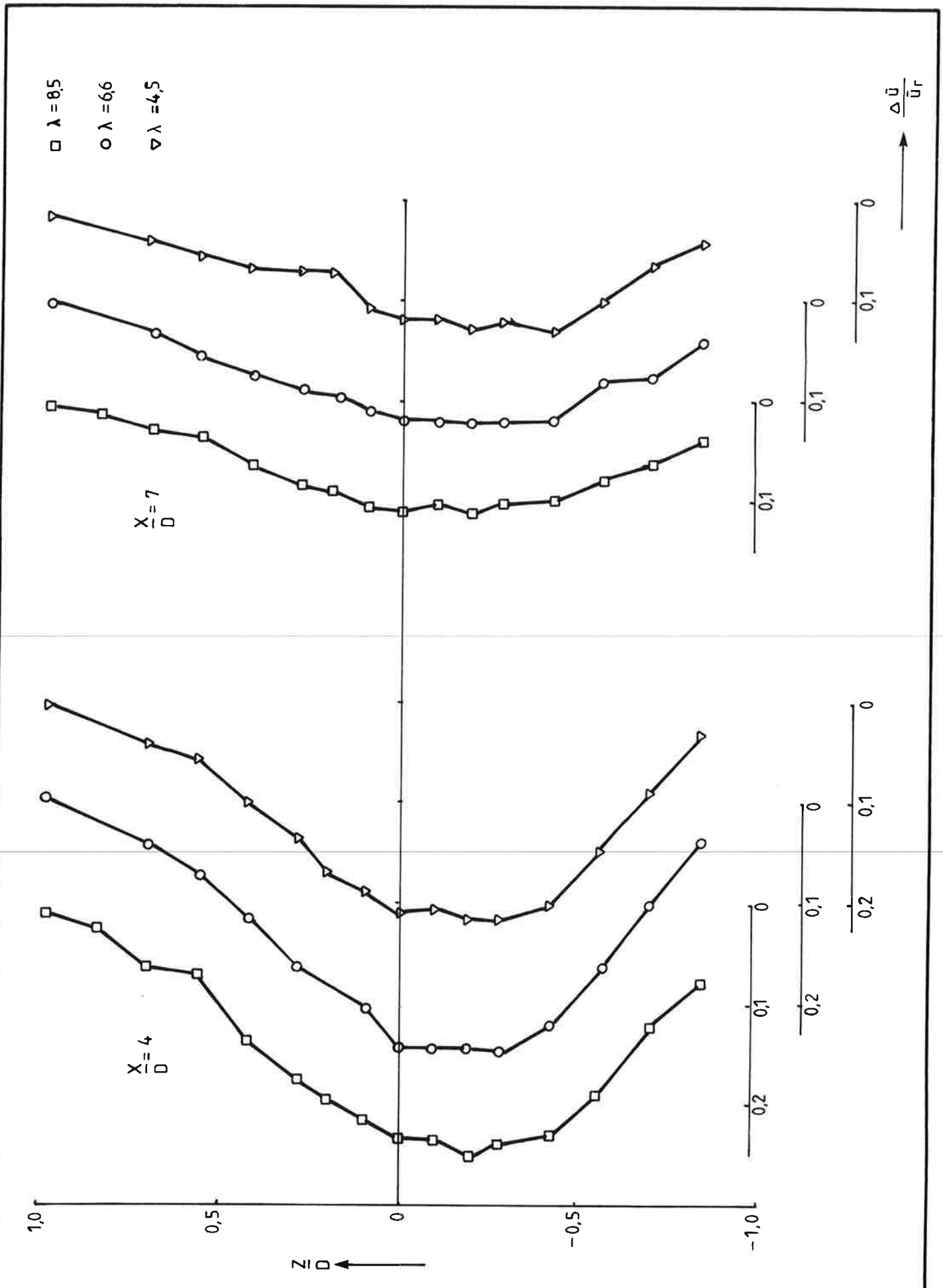

Vertical velocity defect profiles at X/D = 4 and 7

MT_TNO
12433
Fig.24

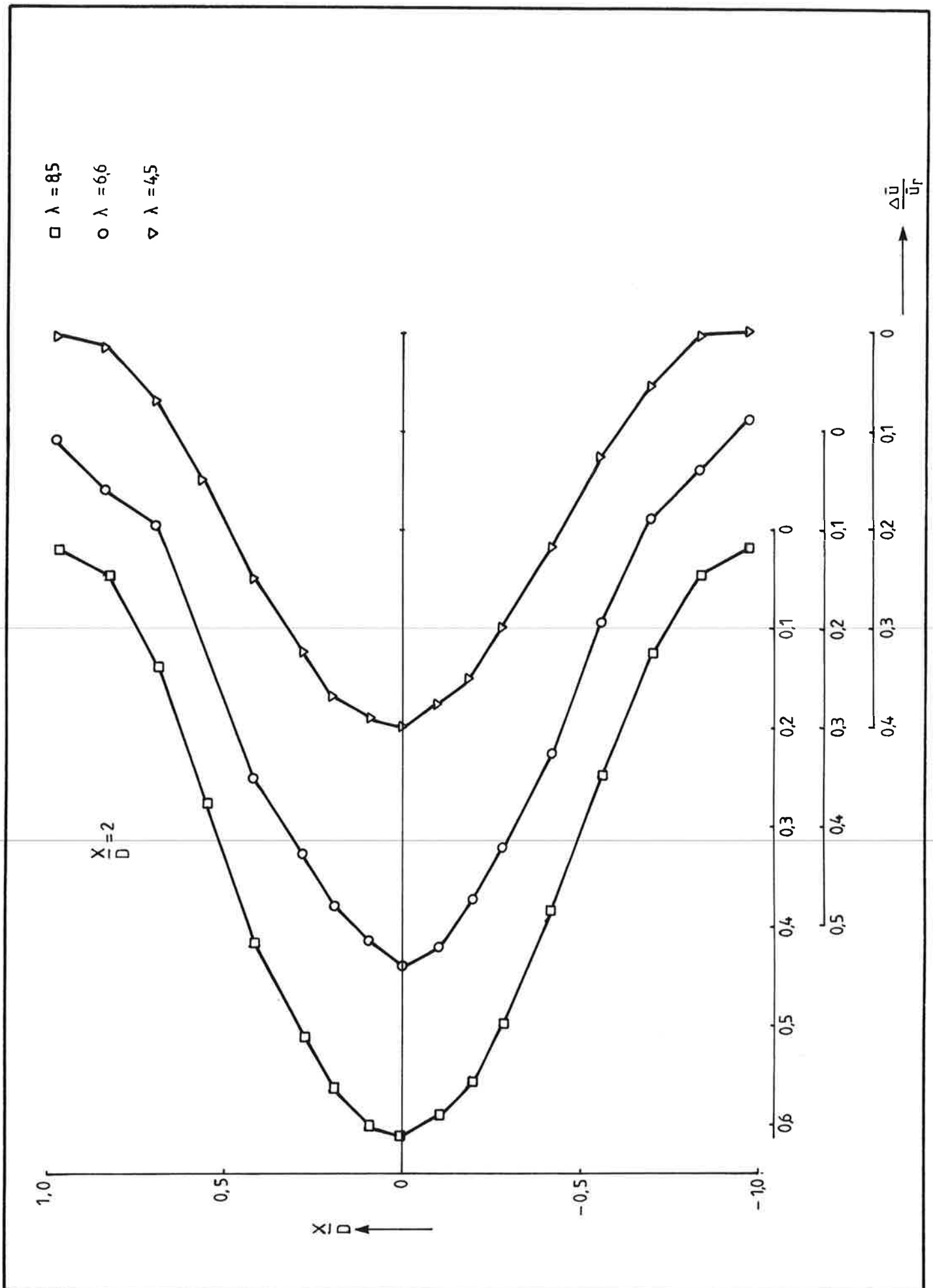

Horizontal velocity defect profiles at X/D = 2

MT_TNO
12433
Fig.25

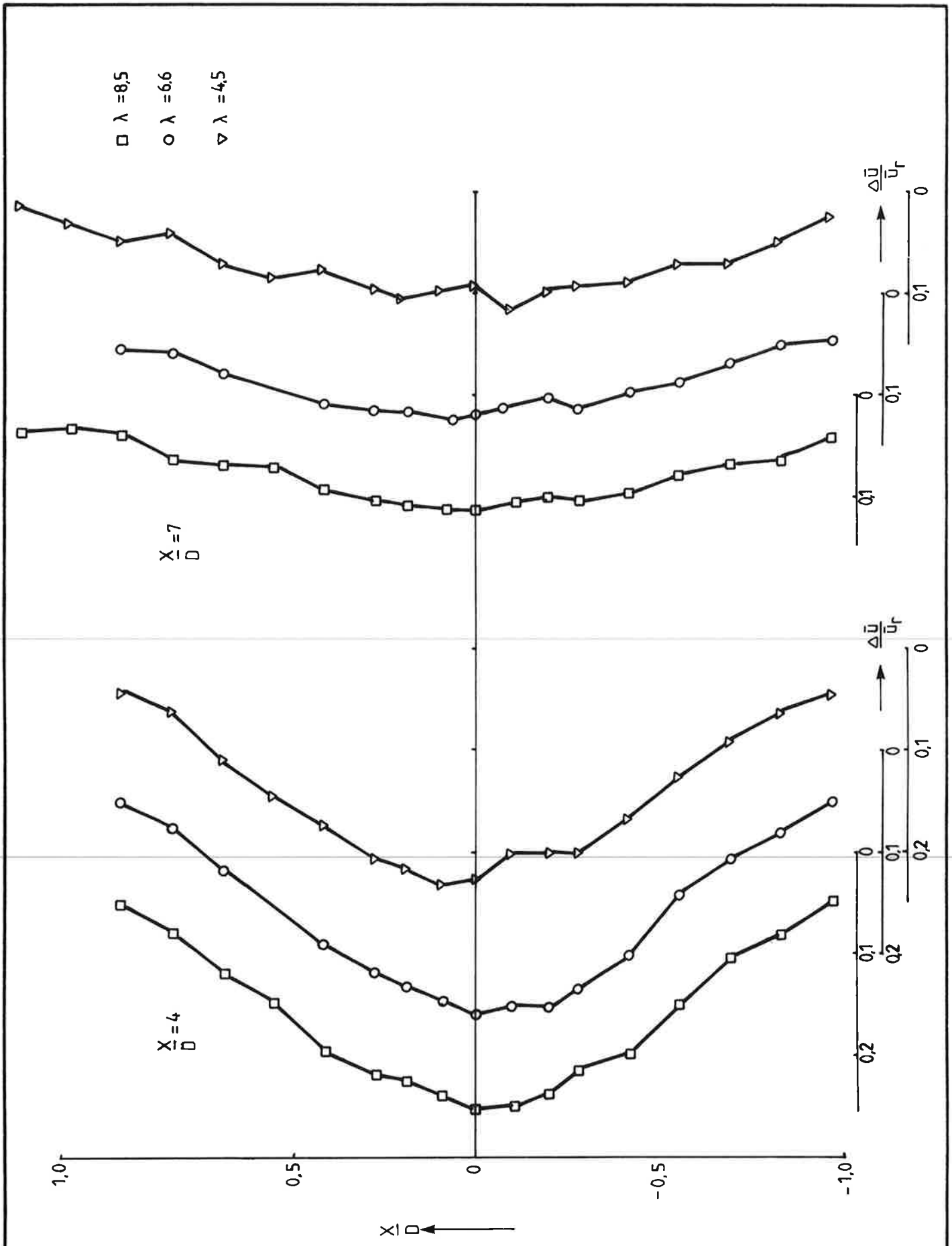

Horizontal velocity defect profiles at X/D =4 and 7

MT_TNO
12433
Fig. 26

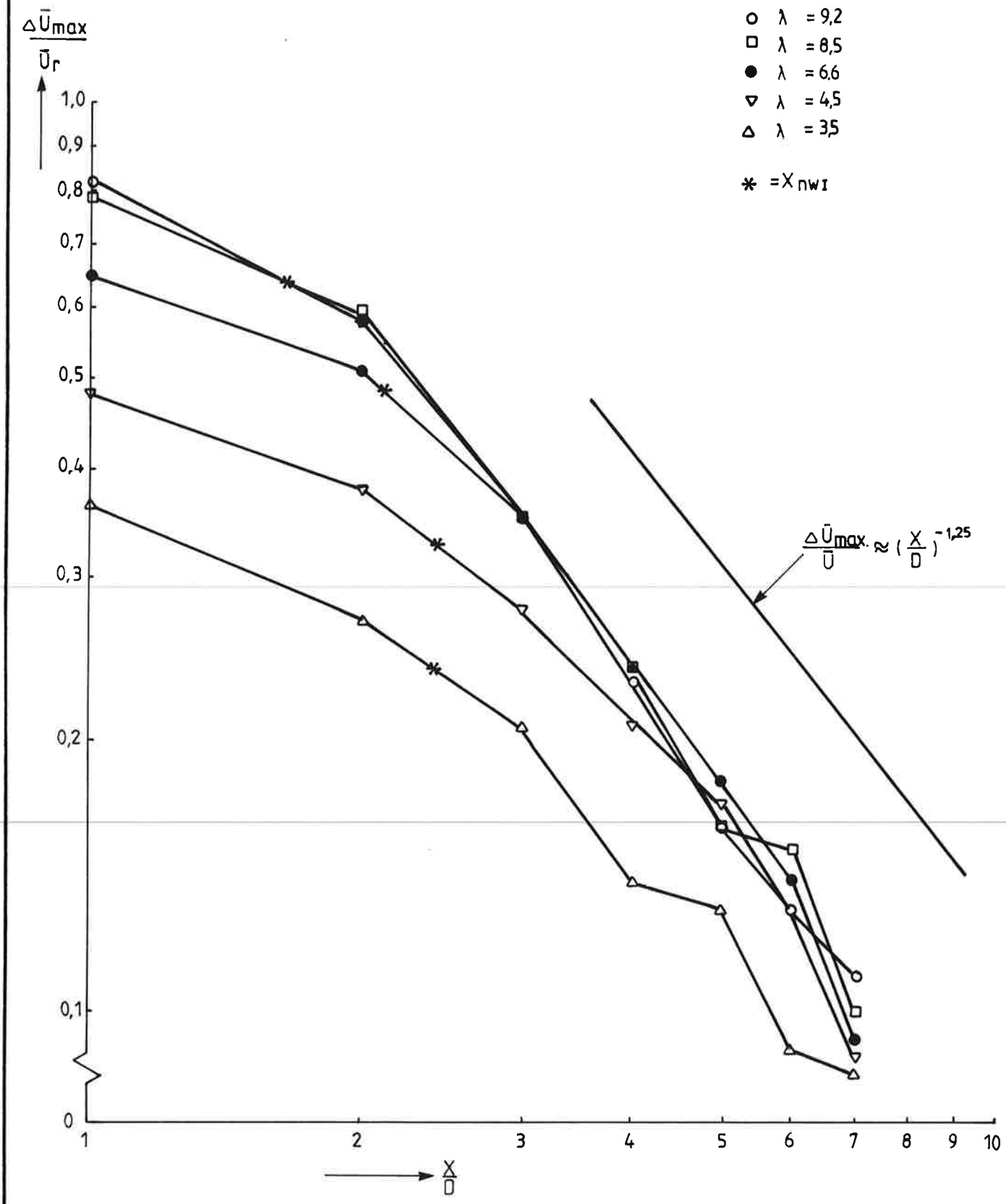

Centerline velocity defect decay

MT_TNO
12433
Fig.27

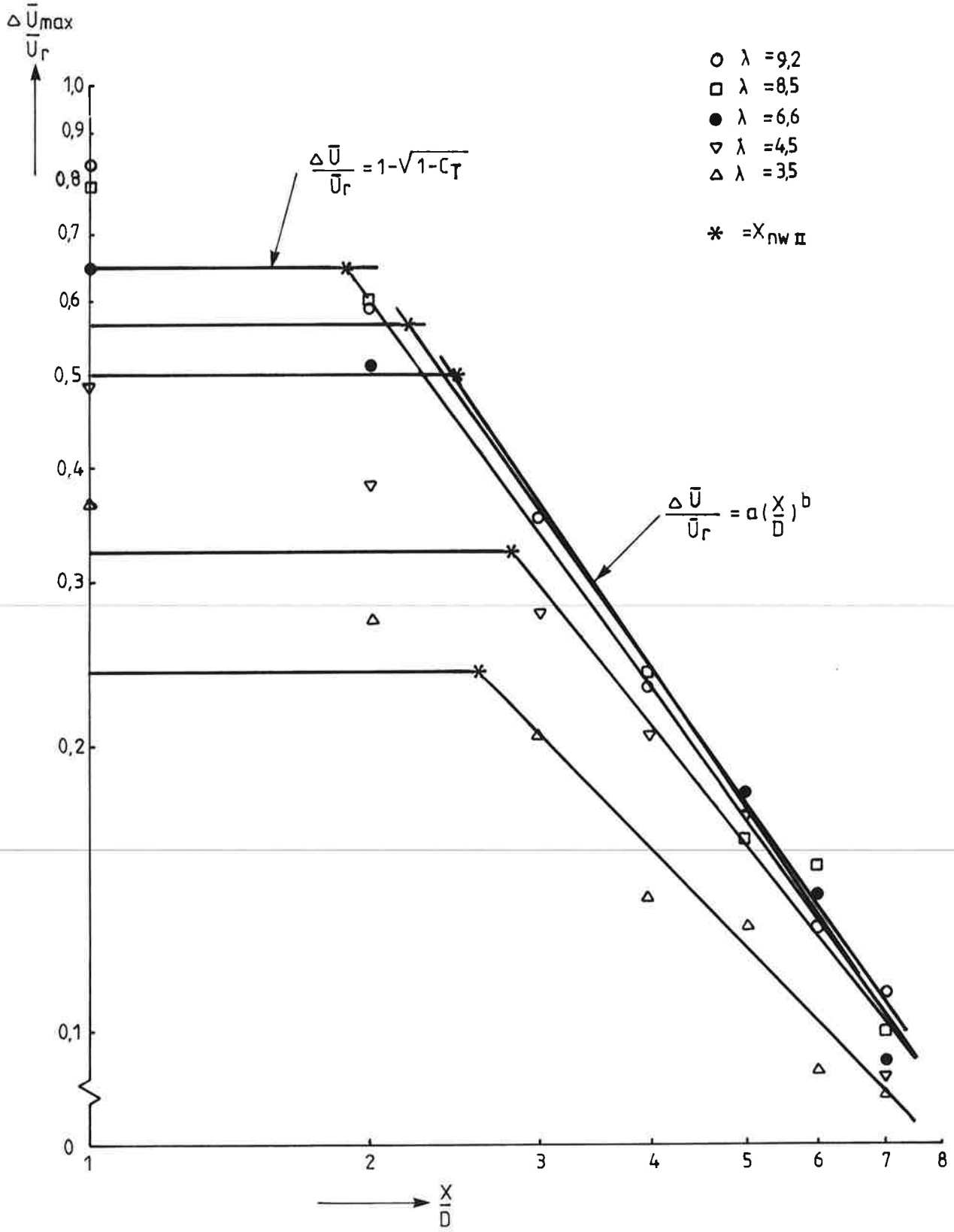

Approximation of centerline velocity defect.

MT_TNO
12433
Fig.28

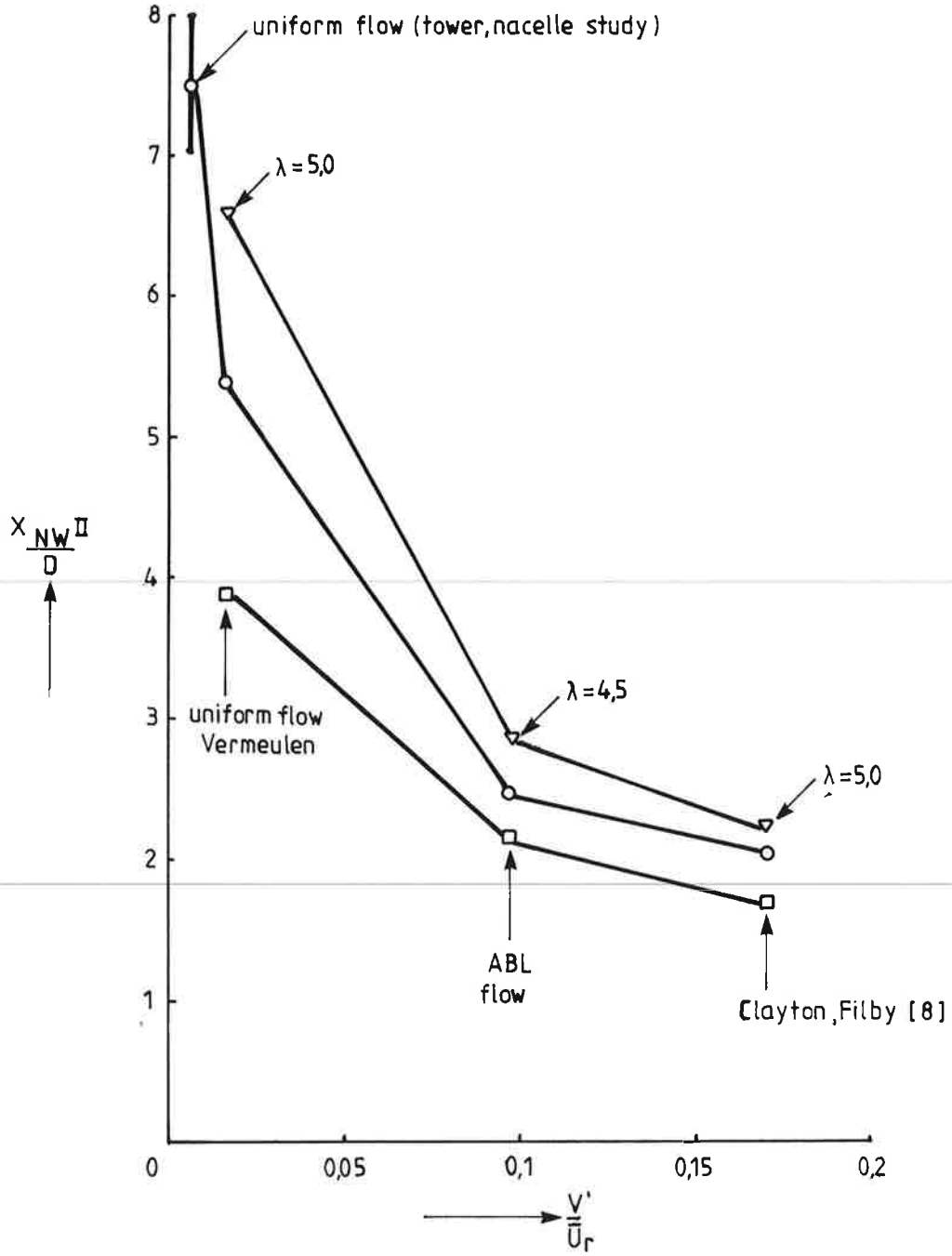

Correlation between turbulence intensity and $X_{NW\,II}$

MT_TNO
12433
Fig.29

Vertical and horizontal turbulence intensity profiles at $\lambda = 6{,}6$

MT_TNO
12433
Fig.30

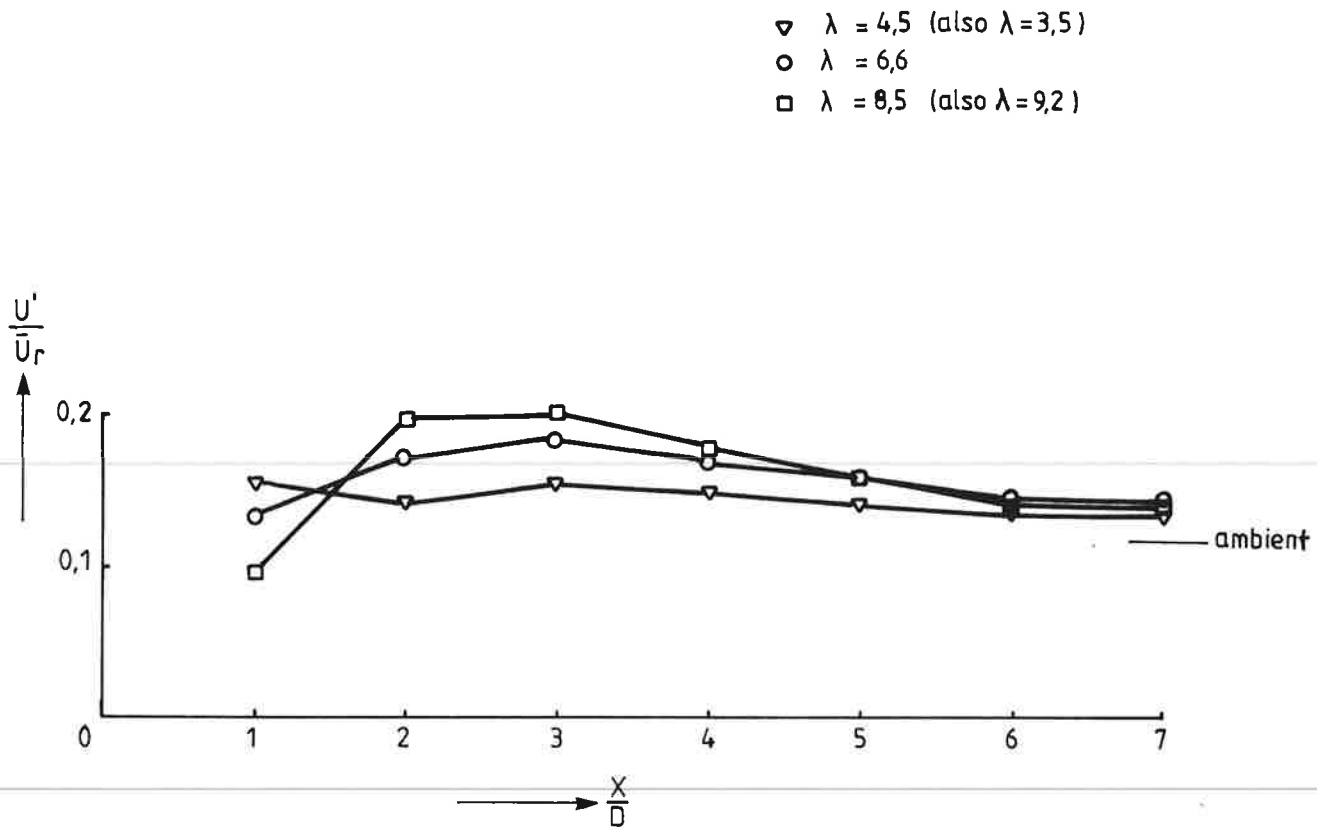

Turbulence intensities on rotorcenterline

MT_TNO
12433
Fig.31

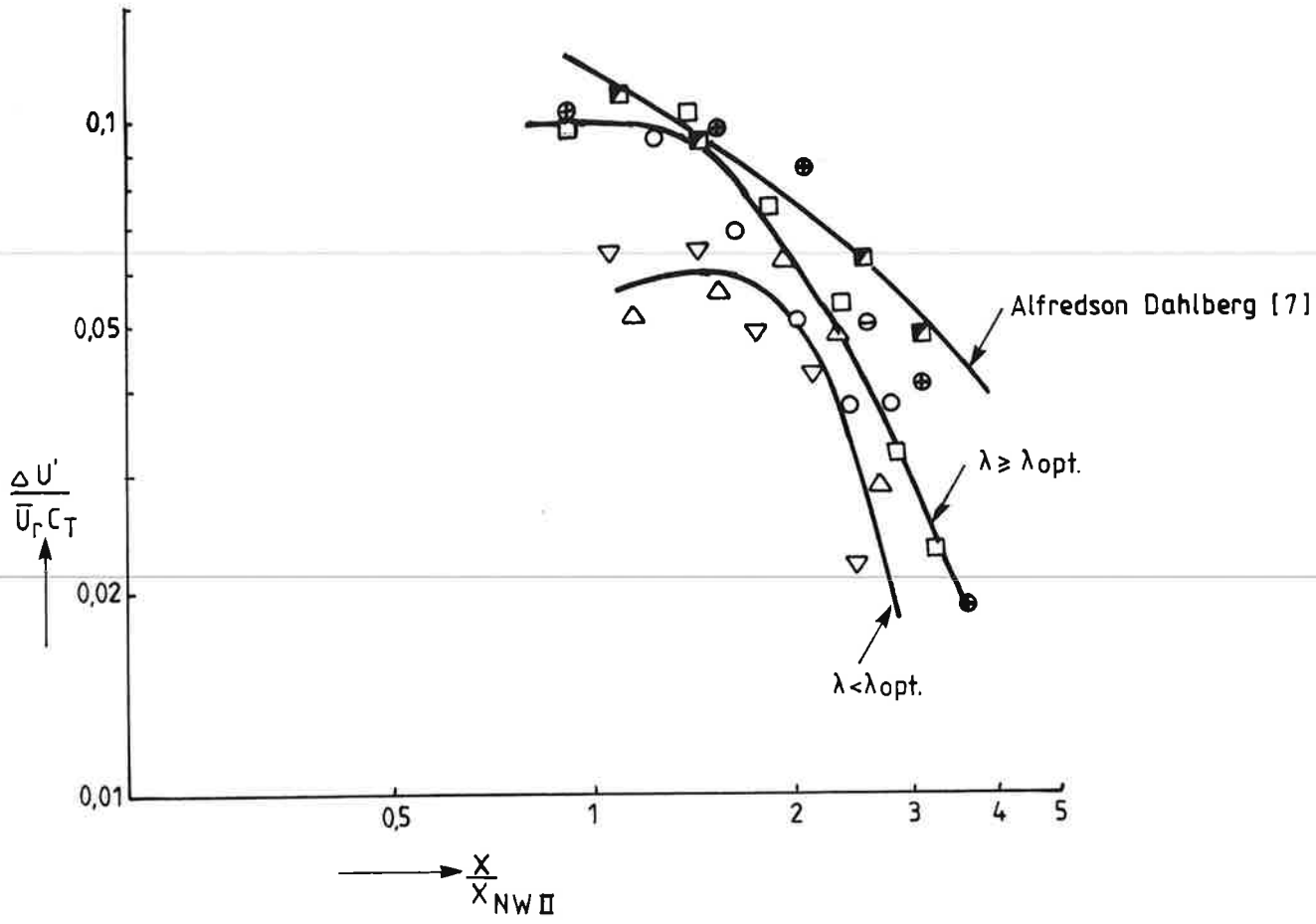

Correlation of centerline turbulence intensity.

MT_TNO
12433
Fig. 32